2018-01-08

Development of a High-pressure Rotational Rheometer for Investigation of Effects of Dissolved CO2

Lee, Keonje

UNIVERSITY OF CALGARY

Development of a High-pressure Rotational Rheometer for Investigation of Effects of Dissolved CO_2

by

Keonje Lee

A THESIS

SUBMITTED TO THE FACULTY OF GRADUATE STUDIES

IN PARTIAL FULFILMENT OF THE REQUIREMENTS FOR THE

DEGREE OF MASTER OF SCIENCE

GRADUATE PROGRAM IN MECHANICAL ENGINEERING

CALGARY, ALBERTA

JANUARY, 2018

Abstract

Rheological information is often used to determine viscoelastic fluid properties, and to model and predict fluid behavior under influence of external stress or deformation. Many industrial processes involve the dissolution of gas under high pressure, so it is important to evaluate the rheological properties of viscoelastic materials under high pressure. In this research, a high pressure rotational rheometer was developed to measure the rheological parameters of viscoelastic fluids and investigate the influence of the dissolution of gases on rheology. The rheometer utilized a piezoelectric torque transducer, which enabled transient and dynamic rheological measurements under high pressure. First, the rheometer was designed, fabricated, and calibrated using a calibration fluid. Second, the capability of the rheometer was verified using polydimethylsiloxane (PDMS), which is a typical viscoelastic fluid. Viscosity and viscoelastic properties, such as storage/loss modulus, and complex viscosity, were evaluated. Thirdly, the effects of the dissolved CO_2 on the rheological properties of PDMS were investigated. The effects of temperature and dissolved CO_2 were investigated individually at the temperature of 25, 50, 80°C and CO_2 saturation pressures of 1, 2, 3 MPa. Then, the combined effect was correlated using a generalized Arrhenius model. The proposed model expressed viscosity as a function of temperature and pressure without the need for thermodynamic and volumetric information of the fluid. The achievement of this research provides an alternative method to measure rheological properties of viscoelastic materials under high pressure and enables the prediction of the viscosity of a fluid with dissolved gas through modelling.

Acknowledgements

The research undertaken for this thesis was conducted at the Mechanical and Manufacturing Engineering department at the University of Calgary. This work would not have been possible without the guidance of Dr. Simon Park, my supervisor who has been supportive of my master's program and career goals. He worked to provide me with continuous guidance, encouragement and support to pursue those goals.

I would like to thank the supervisory committee members, Dr. Seonghwan Kim and Dr. Joanna Wong, and external examiner, Dr. Giovanniantonio Natale for taking the time to review this thesis. I would especially like to thank Dr. Giovanniantonio Natale for his professional guidance in this research.

I am grateful to all of those with whom I have had the pleasure to work with during this program. I would like to express my gratitude to my colleagues at the Micro Engineering Dynamics and Automation Lab (MEDAL) for their assistance and friendship. I would especially like to thank Mr. Allen Sandwell, Dr. Changyong Yim, Dr. Jongho Won, and Mr. Chaneel Park for their assistance and support.

Dedicated to my parents in Korea and Canada, my fiancé Gabrielle, and my sisters Jieun, Ann and Yun for their love, endless support and sacrifices

Table of Contents

List of Tables

List of Figures

List of Symbols

a_c	Concentration shift factor
a_p	Pressure shift factor
A	Constant
A'	Constant
B	Constant
B'	*Constant*
C	Constant
C_1	WLF parameter
C_2	WLF parameter
d	Distance from the center of the torque dynamometer
e	Bagley end correction
E_0	Activation energy for flow
E_s	Enthalpy of dissolution
F	Force measured by impact hammer
f	Fractional free volume
f_m	Fractional free volume of polymer-gas mixture
f_p	Fractional free volume of pure polymer
g	Gravitational acceleration
G	Spring constant
G'	Storage modulus (elastic modulus)
G''	Loss modulus (viscous modulus)
G^*	Complex modulus
G_0	Relaxation constant
$\|G^*\|$	Magnitude of complex modulus
h	Distance between plates
H	Henry's solubility constant
L	Length of cylinder
L_0	Length of capillary
M	Torque
M_0	Torque measured on the outer cylinder
M_c	Torque contribution at the wall of the cylinder
M_{fluid}	Torque caused by shearing of the fluid
$M_{friction}$	Torque caused by the friction between the seal and the shaft
$M_{measured}$	Measured torque
M_p	Torque contribution at the bottom of the cylinder
M_{tot}	Total torque
n	Constant
N_1	First normal stress difference
N_2	Second normal stress difference
P	Pressure
P_d	Pressure drop in capillary
$\tilde{P}$	Reduced pressure

q	Effective polymer chain length
Q	Flow rate
R	Gas constant
r	Number of lattice sites occupied by a polymer chain
R_b	Radius of the ball
R_c	Radius of the capillary
R_i	Radius of the inner cylinder
R_o	Radius of the outer cylinder
T	Temperature
t	Time
t'	Past time variable
T_0	Reference temperature
T_{fluid}	Temperature of fluid
T_r	Constant
T_{sp}	Temperature set-point
$\tilde{T}$	Reduced temperature
v_∞	Terminal velocity
$\tilde{v}$	Reduced volume
V_m	Specific volume of polymer-gas mixture
V_p	Specific volume of pure polymer
w_c	Weight fraction of dissolved gas
x	Deformation at the top lane of a rectangular parallelepiped geometry
y_0	Height of a rectangular parallelepiped geometry
Z	Coordination number of the lattice
α	Constant
β	Constant
γ	Strain
γ_0	Amplitude of strain
$\dot{\gamma}$	Shear rate
$\dot{\gamma}_A$	Apparent shear rate for a Newtonian fluid
$\dot{\gamma}_w$	Shear rate on the wall
δ	Phase difference
η	Viscosity (damping constant)
η_0	Viscosity at a reference temperature
η_{0,w_c}	Viscosity of pure polymer
η_z	Zero-shear viscosity
$\lvert\eta^*\rvert$	Magnitude of complex viscosity
θ	Parameter representing contribution of dissolved gas
λ	Relaxation time
ρ_b	Density of the ball
ρ_f	Density of the fluid
$\tilde{\rho}$	Reduced density
τ	Shear stress
τ_0	Amplitude of stress
τ_w	Shear stress on the wall

ψ	Constant
ψ_1	Normal stress coefficient
ψ_2	Normal stress coefficient
ω	Angular frequency
Ω	Angular velocity

CHAPTER 1: INTRODUCTION

Rheology is the study of stress and deformation of matter. It is an interdisciplinary field that crosses over physics, chemistry, and several other disciplines. In fact, rheology is a fundamental study that governs the mechanical deformation and flow of all pure and mixed materials. There are various rheological parameters including viscosity, relaxation modulus, storage modulus, loss modulus, complex viscosity, creep compliance, etc. Among these rheological parameters, viscosity is the most widely used parameter, especially when flowability of a material is a primary concern. It is well known that the viscosity of fluids is a critical parameter in the hydraulic calculations of various systems including surface facilities, pipeline systems, and flow through porous media (Monnery et al. 1995). Although viscosity provides information on how fluids flow under steady shear, it does not sufficiently provide all the necessary information to fully describe complex material behaviors under the transient or dynamic change of strain or stress.

Response of viscoelastic materials under external stress or deformation is characterized by rheological parameters such as relaxation modulus/spectrum and dynamic modulus. The relaxation modulus is a measure of material response under transient strain over time. It has been reported that the stress relaxation spectrum, which is a distribution of relaxation times, can be used to estimate the molecular weight distribution by making assumptions in terms of the functional relationship between molecular weight and relaxation time (Marin and Montfort 1996). It is one of the fundamental ways to determine the viscoelasticity of materials; however, the use of stress relaxation is limited to materials that have relatively long relaxation times due to experimental challenges such as difficulty in measuring stress over time. The dynamic modulus,

which can be obtained from oscillatory measurements, is another important viscoelastic function that is interchangeable with relaxation modulus. Both dynamic and relaxation modulus, as well as other viscoelastic parameters, are correlated to one another and convertible to each other when mathematical calculations are applied. By using these parameters, the molecular structure of thermoplastic melts can be identified (Rohn 1995), and the crosslinking process of thermosetting polymers can be monitored (Calvet et al. 2004). In other words, the aforementioned parameters allow scientists and engineers to gain a fundamental understanding of the micro-structure and flowability of materials.

Rheometers are instruments that measure the rheological parameters of materials, which are fluids in most cases. They evaluate these parameters by measuring the stress induced as a response to an applied strain or vice versa. Rheometers can be classified into two major categories based on the way shear flow is generated: pressure drop and drag flow rheometers. Pressure drop rheometers include capillary rheometers and slit-die extrusion rheometers. They are used in processes where the shear is induced by pressure. Drag flow rheometers include falling ball, parallel plate, and rotational rheometers. One major advantage of using a falling ball rheometer is the simplicity of the system and the ease of applying high static pressure. However, there is also a major disadvantage of this system: it is difficult to control stress and strain due to the fixed dimensions and mass of the ball. Moreover, the flow field induced by the ball is very complex causing difficulties in analyzing the flow. Rotational rheometers are the most versatile types of rheometer because various stress or strain profiles can be imposed on a sample by displacing the surface that is in contact with the sample. These are thus more suitable for dynamic or transient measurements.

The development of various rheometers and advanced rheological techniques have deepened the understanding of the flow properties of various fluids. Some of the industrial sectors that benefit from these advancements include polymer/plastic, coatings/paints, oil/petrochemical, geoscience, biomedical, and pharmaceutical industries. The heavy oil industry is one of the major applications because the processes involved in the industry is largely affected by the flow properties of heavy oil. Heavy oil does not flow as easily compared to other light crude oils, thus posing several difficulties in terms of extraction from reservoirs and transportation through pipelines.

Recently, injecting carbon dioxide (CO_2) into a heavy oil reservoir has been drawing attention in enhanced oil recovery due to its environmental and economic advantages. In addition to displacing heavy oil from reservoir rock by building up pressure within the reservoir, injecting CO_2 also improves the rheological behavior of heavy oil by dissolving into the heavy oil under high pressure. CO_2 is highly soluble in heavy oil and is effective in viscosity reduction by dissociating the micro-structure in heavy oil. Therefore, it is necessary to understand the rheological behavior of heavy oil under high pressure and in the presence of dissolved CO_2 to optimize the process and better understand the micro phenomena associated with the dissolution of CO_2.

1.1 Motivations

Measuring the rheological parameters is essential in heavy oil industries because these parameters are closely related to the flow of heavy oils. The most fundamental use of the rheological data is to construct a mathematical model that describes the relationship between the flow (deformation) and applied stress. This model is called a constitutive equation and can

predict the response of heavy oil under various histories of shear deformation. For example, the linear and nonlinear viscoelastic behaviors of heavy oil have been modeled using constitutive equations with rheological data collected from dynamic and stress relaxation experiments (Behzadfar and Hatzikiriakos 2013). Rheological parameters also provide information on the structure of heavy oil and how the structure affects the flow and vice versa. Many studies have revealed that the intermolecular aggregation of asphaltene molecules are the major factor contributing to the poor flowability of heavy oil, and the aggregation can be dissociated by adding organic solvents or soluble gases (Pierre et al. 2004). Therefore, accurate and reliable measurements of rheological parameters are of great importance.

Among the various type of rheometers, rotational rheometers are the most versatile and able to perform various rheological measurement including dynamic measurements. For high pressure applications, a magnetic coupling drive is often utilized to ensure the sample is completely sealed off from the atmosphere, while torque is transferred to the rheometers. This type of rheometer can eliminate the problems related to pressure gradients and non-homogeneity within a sample because constant pressure throughout the sample can be achieved. Moreover, because the flow field is known, shear stress and strain can be directly calculated from the geometry and dimensions of the rheometer. Another advantage is that stress and strain are easily manipulated by simply changing the speed or profile of the rotation. Various rheological tests can be performed using rotational rheometers including steady shear, sinusoidal oscillation, stress relaxation, and creep recovery. Although there are several advantages, these rheometers are often difficult to design and fabricate. One of the main difficulties is in measuring the dynamic torque. Torque is a primary measured variable in rotational rheometers and an accurate measurement of torque is essential for accurate rheological measurements.

Traditionally, torque has been measured using a torsion bar/spring. The amount of deflection of the torsion bar/spring is measured using a strain gauge. This method is still widely used in rotational rheometers due to its simplicity and high sensitivity depending on the stiffness of the bar/spring. The main drawback of the torsion bar/spring is that the deflection of the torsion bar/spring causes an error in the strain imposed on the sample. Moreover, the low rigidity can lead to a delay in the response to the applied strain and low resonance frequency; this delay can result in a reduced range of transient or dynamic rheological testing. The problem of transducer deflection can be eliminated by using a feedback control servo. The amount of current needed to rotate the motor is proportional to the torque exerted on the fluid. However, the servo system requires some time for feedback, which causes a delay in the torque measurement. Fast acceleration or deceleration of the motor can also result in inaccurate torque measurements due to the inertia of the motor and the spindle/shaft. Therefore, a torque measurement technique for rotational rheometers that is more suitable for dynamic measurements should be explored.

Considering the limitations of the current high pressure rotational rheometers, using a structurally rigid torque transducer with minimum inertial effect can significantly improve the range of dynamic rheological measurements in rotational rheometers.

1.2 Objectives

The goal of this study is to investigate a new method to take rheological measurements of viscoelastic fluids under high pressure that also involves the dissolution of a gas. This goal is achieved by meeting the following specific aims:

i. Development of a rotational rheometer with a piezoelectric torque transducer

A rotational rheometer was designed, fabricated, and calibrated to measure the rheological properties of viscoelastic fluids. The concentric cylinder is driven by a brushless DC motor to impose the desired strain or strain rate exerting torque on the fluid in the rheometer. Torque is measured using a piezoelectric torque transducer, which has a number of advantages over other types of torque measurement techniques. First, it is rigid and, thus, has a higher frequency bandwidth, resulting in more accurate measurements, especially in terms of dynamic measurements. Second, the charge signal, which is the output of the transducer, is strictly proportional to the load over a wide torque range.

Therefore, a wide range of dynamic viscosities can be accurately measured using the piezoelectric torque transducer. The developed rheometer is equipped with a high pressure dynamic shaft seal, which can be pressurized up to 3 MPa in the concentric cylinder; additionally, a band heater is utilized to control the temperature up to 300°C. The developed rheometer is calibrated using a calibration fluid to convert the torque to a corresponding shear stress.

ii. Investigation of rheological behavior of polymer melts

The capability of the developed rheometer is verified using a calibration fluid and PDMS under ambient temperature and pressure. These two fluids represent a Newtonian fluid and a non-Newtonian fluid that exhibit viscoelasticity. Their rheological behaviors are well known, and therefore, they are used for the purpose of validation. Rheological measurements are performed in steady shear and sinusoidal oscillation modes. In steady shear mode, shear stress is measured at various shear rates and the shear viscosity is determined. In sinusoidal oscillation mode, the amplitude of shear stress and phase difference are measured and the dynamic

rheological parameters, including storage modulus, *G'*, loss modulus, *G''*, and complex viscosity, $|\eta^*|$, are determined. Strain sweep tests are performed to determine the linear viscoelastic range of PDMS, and frequency sweep tests are also performed to evaluate the dynamic rheological parameters. Methods to compensate for the friction of the shaft seal are proposed, and the results are compared to tests conducted without the shaft seal.

iii. Investigation of the effect of dissolved CO_2 on the rheology of polymer melts and validation through modeling

The effects of temperature, pressure, and dissolved CO_2 on the rheological properties of PDMS are investigated using the developed rheometer. Steady shear measurements are carried out first at ambient pressure (without CO_2) and various temperatures. Then, the effect of pressure (thus, CO_2 concentration) on viscosity is experimentally investigated at different temperatures. After examining the effect of the individual parameters, the experimental results are then correlated to a generalized Arrhenius model. Using this model, viscosity can be mathematically expressed as a function of temperature and pressure without the need for thermodynamic information, which is difficult to measure. Sinusoidal measurements are also conducted to evaluate dynamic rheological parameters under the same conditions as the steady shear measurement.

Through the completion of these objectives, a rheometer that can operate in pressurized conditions will be developed. The developed rheometer will also be capable of performing various rheological measurements in an increased dynamic range. The measurement error associated with the compliance and inertia of torque transducers will be minimized. In addition,

the effect of various conditions, including temperature, pressure, and concentration of CO_2, on rheological parameters can be evaluated and predicted using the proposed model.

1.3 Thesis Organization

This thesis consists of five chapters including the introduction and is organized as follows:

Chapter 2 provides some theoretical background on rheology and the concept of linear viscoelasticity. Various rheological measurement techniques and equations are also discussed. Free volume theory and several predictive models based on this theory are introduced. Some of the recent research on the development of rotational rheometers are summarized along with their limitations.

The development of a high pressure rotational rheometer is described in Chapter 3. The overall design and major sub-components of the rheometer are described in detail. A detailed description of the rheological measurements, calculations, and friction compensation schemes are presented. Some of the results of the preliminary tests using a calibration fluid and PDMS are also presented.

The rheological properties of PDMS are investigated in Chapter 4 using the developed rheometer. The effect of temperature and dissolved CO_2 on the rheological parameters of PDMS are studied in steady shear mode. Modeling of the viscosity using an empirical model is presented in detail. The dynamic modulus (G' and G'') and complex viscosity (η^*) are experimentally determined.

The last chapter, Chapter 5, concludes the presented work. A summary of the thesis and a brief discussion of the results are provided. The novel contributions in the area of rheometer

development are discussed, followed by an explanation of the limitations and assumptions of the presented work. This chapter concludes with recommendations for possible future work.

CHAPTER 2: LITERATURE SURVEY

In this chapter, the theoretical background on rheology is presented and relevant works on rheometer development and high pressure rheology are reviewed. The difference between Newtonian and non-Newtonian fluids is presented as well as the basic concepts and theoretical background of linear viscoelasticity. Two rheological measurement techniques: steady shear and sinusoidal oscillation, are described along with the rheological parameters that can be evaluated using these techniques. Then, various types of rheometers, including ones that have been designed or modified to accommodate high pressures, are introduced, and their pros and cons are discussed. Experimental and theoretical studies on the effect of dissolved gas on viscosity reduction are also discussed along with their associated predictive models.

2.1 Viscoelasticity of Materials

Rheology is the study of flow and deformation of materials under the influence of stresses. It is often used to determine fluid properties and predict the behaviour of fluids. With the recent wide-spread use of polymeric fluids, it is critical to achieve a method to study the deformation and flow behaviours of time-dependent, semi-solid, or viscoelastic fluids. Viscoelastic behaviour should be studied to expand our knowledge of the wide range of material behaviours and the ultimate product performance.

Isaac Newton addressed the problem of steady flow in late 17^{th} century in his famous *Principia Mathematica*, which contains the hypothesis: "the resistance which arises from the lack of slipperiness of the parts of the liquid, other things being equal, is proportional to the velocity with which the parts of the liquid are separated from one another." Newton's "lack of

slipperiness" is now called viscosity. This concept is now scientifically described using shear stress (τ) and shear strain (γ). A rectangular parallelepiped geometry, shown in Figure 2.1, is subjected to a shear stress at the top plane while the bottom plane is stationary. The shear stress the successive layer of the material to deform. Here, shear strain is defined as follows:

$$\gamma = \frac{x(t)}{y_0} \tag{2.1}$$

where the height is y_0 and deformation at the top plane is $x(t)$. The rate of change in shear strain is defined as strain rate ($\dot{\gamma}$) and can be expressed as:

$$\dot{\gamma} = \frac{d\gamma}{dt} \tag{2.2}$$

Then, viscosity can be defined by the following mathematical expression:

$$\eta = \frac{\tau}{\dot{\gamma}} \tag{2.3}$$

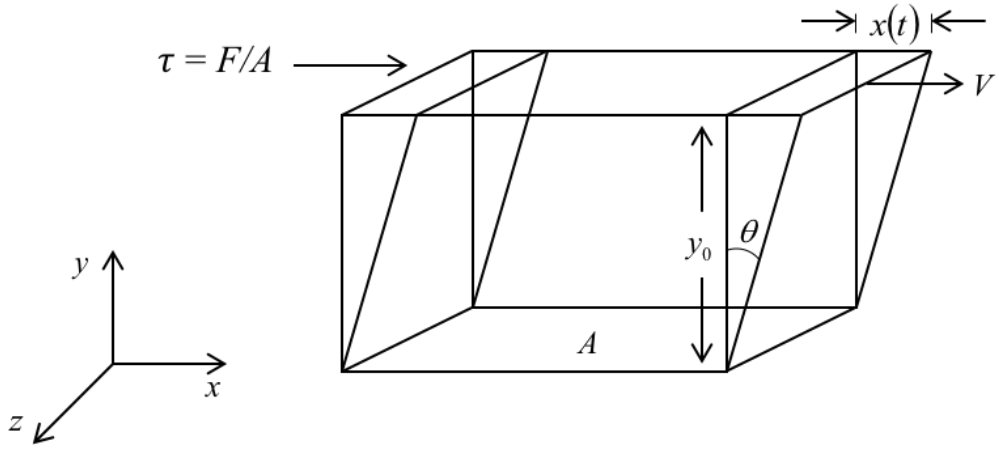

Figure 2.1 Shear deformation

2.1.1 Newtonian and Non-Newtonian Fluids

Fluids can be classified as Newtonian or non-Newtonian depending on their shear stress response to shear rate. Most fluids with a low molecular mass, such as water, organic solutions, or gases, exhibit the characteristic that the shear stress is directly proportional to the shear rate at a given temperature and pressure, leading to a constant viscosity. These fluids are classified as Newtonian, named after Isaac Newton who first derived the relation between shear stress and shear rate.

The most obvious deviation from Newtonian fluid behavior is that the flow curve does not pass through the origin and/or is no longer linear. Therefore, for non-Newtonian fluids, the viscosity, the slope of the flow curve, is not constant; rather it is a function of shear rate or shear stress. Studies have also shown that the viscosity of a non-Newtonian fluid can depend on the kinematic history of the fluid. These fluids are conveniently grouped into three general classes. The first one includes the fluids whose shear rate, at any position of the fluid, is related only to the value of the shear stress at that position at any given time. These fluids are usually called "time-independent" fluids. The second class is for more complex fluids whose relationship between shear stress and shear rate is a function of time, and they are called "time-dependent" fluids. Finally, the third class is for the fluids that behave as a fluid under shear but as an elastic solid at rest (infinite viscosity). They are categorized as "visco-plastic" fluids. Most real materials illustrate a combination of these features under certain conditions.

2.1.2 Linear Viscoelasticity

Viscoelastic materials are materials whose relationship between stress and strain is time-dependent. For example, when materials like silk, rubber, or glass are loaded in shear or

extension, an instantaneous deformation is followed by a continuous deformation (also known as "creep"). When the load is removed, part of the deformation instantly recovers; some materials completely recover with time, and other materials do not recover at all. Viscoelastic behavior is typical of all polymeric materials. It is common to measure this phenomenon using stress relaxation. An illustration of the behavior of viscoelastic materials compared to other materials is shown in Figure 2.2.

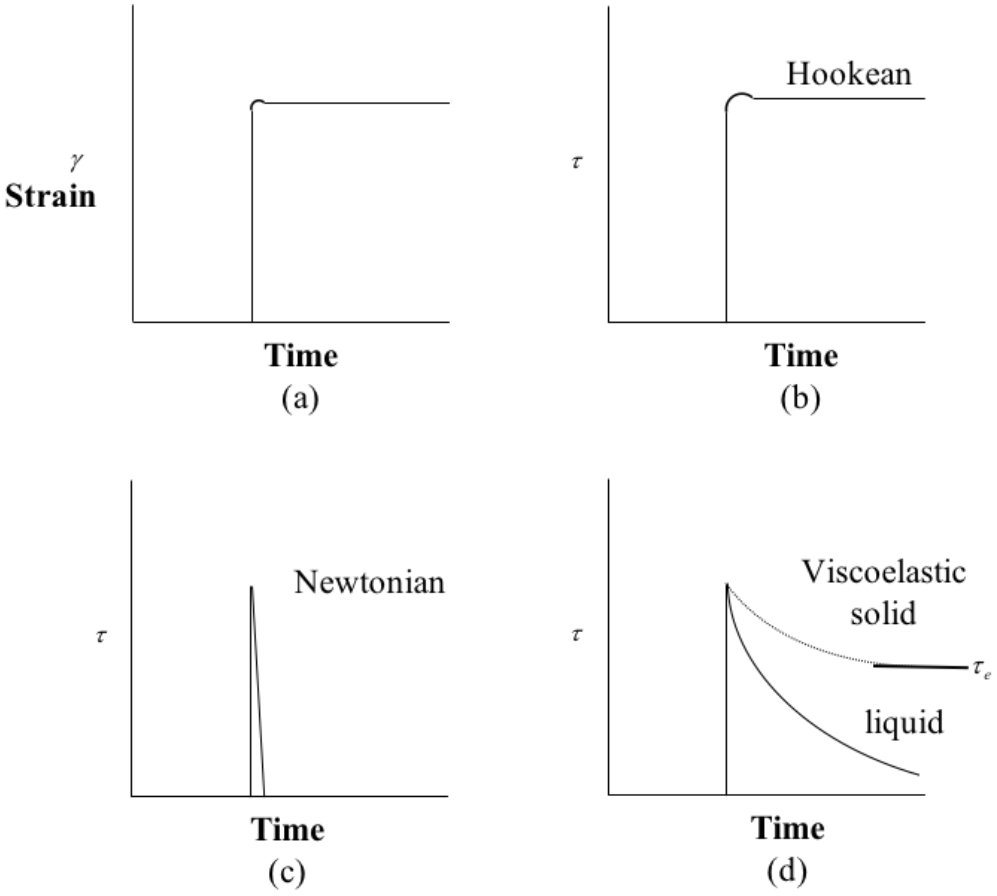

Figure 2.2 Stress response τ vs. time for step input in strain γ

Figure 2.2 (a) shows the step input in strain, and figures 2.2 (b), (c), and (d) show the stress response for different materials as a function of time. The Hookean solid (b) shows no

stress relaxation, and the Newtonian fluid (c) relaxes as soon as the strain is constant. In addition, the viscoelastic material (d) shows stress relaxation over time. In a viscoelastic liquid, the stress relaxes to zero, while in a viscoelastic solid, the stress approaches an asymptotic value (known as equilibrium stress).

Linear viscoelastic materials display a linear relationship between stress relaxation and strain at any given time. Linear viscoelasticity is a theory that describes the behavior of such ideal materials. This theory is a reasonable approximation of the time-dependent behavior of polymers, metals, and ceramics at relatively low temperatures and under relatively low stress. For larger strains, the relaxation modulus is no longer independent of strain.

2.1.3 Linear Viscoelastic Models

Viscoelastic materials have properties of both viscous and elastic materials, represented by Newtonian liquids and Hookean solids, respectively. Therefore, it is a reasonable approach to express viscoelastic material responses as a combination of a dashpot and spring. This concept has been the basis of various mechanical models of linear viscoelasticity. Stress (τ) of viscous liquids and elastic solids in response to strain (γ) can be expressed as follows:

$$\tau = \eta\dot{\gamma} \tag{2.4}$$

$$\tau = G\gamma \tag{2.5}$$

where η is the coefficient of viscosity and G is the shear modulus that have analogies with damping and spring constant, respectively. If a dashpot and a spring are connected in parallel, the total stress is the sum of the contributions of each element:

$$\tau = \eta\dot{\gamma} + G\gamma \tag{2.6}$$

The above equation is one of the simplest forms of a mechanical model called the Voigt model. Another simple form is the Maxwell model where a dashpot and a spring are connected in series. Then, the total strain rate (or strain) is the sum of the contributions of each element:

$$\tau + \frac{\eta}{G}\frac{d\tau}{dt} = \eta\dot{\gamma} \tag{2.7}$$

Other mechanical models are basically combinations of the Voigt and Maxwell models with a spring and/or dashpot in series and/or parallel. For example, Zener (1944) proposed a three-element mechanical model where a spring is added to the Voigt model in series or to the Maxwell model in parallel. The Burger model is obtained by adding a spring or dashpot to the Zener model. Almost an infinite number of models can be constructed by combining dashpots and springs in various arrangement. However, one model that fits a certain material quite well may not fit other materials. A more general model to represent the viscoelasticity of a material can be constructed by connecting several Maxwell models in parallel, which is called the generalized Maxwell model.

A single Maxwell model, which is given by the differential equation (2.7), can also be expressed in the following form:

$$\tau(t) = \int_{-\infty}^{t} G_0 e^{-(t-t')/\lambda}\dot{\gamma}(t')dt' \tag{2.8}$$

where G_0 is a relaxation constant, t' is a past time variable, and $\lambda = \eta/G$ is a relaxation time. Then, the generalized Maxwell model with N number of Maxwell elements is expressed as the sum of the single Maxwell models as follow:

$$\tau(t) = \int_{-\infty}^{t} \sum_{k=1}^{N} G_k e^{-(t-t')/\lambda_k}\dot{\gamma}(t')dt' \tag{2.9}$$

This expression is useful in modeling most of the polymeric liquids and many other viscoelastic materials. Although the individual elements may not have direct physical relation with the real material, the combination of the elements can describe the linear viscoelastic behavior of material quantitatively without the difficulties of going into mathematic in detail (Barnes et al. 1991).

2.2 Rheological Measurement Techniques

There are various ways to determine and measure the rheological properties of materials using simple techniques. In this section, two rheological measurement techniques, steady shear and sinusoidal oscillation, are discussed. These techniques are related to rheological parameters such as viscosity, normal stress coefficients, storage and loss modulus, and complex viscosity.

2.2.1 Steady Shear

Steady shear flow is characterized by a continuously sheared fluid movement in one direction as shown in Figure 2.3. A shear stress is generated as a response to the shearing, and viscosity η can be calculated as follows:

$$\eta = \tau / \dot{\gamma} \tag{2.10}$$

where τ is the shear stress, and $\dot{\gamma}$ is the shear rate. Viscosity can be expressed as a function of shear rate and from this relationship, Newtonian and non-Newtonian behaviours, such as shear thinning and thickening and yield stress, are distinguished. However, the viscous and elastic responses of materials cannot be distinguished using this measurement technique.

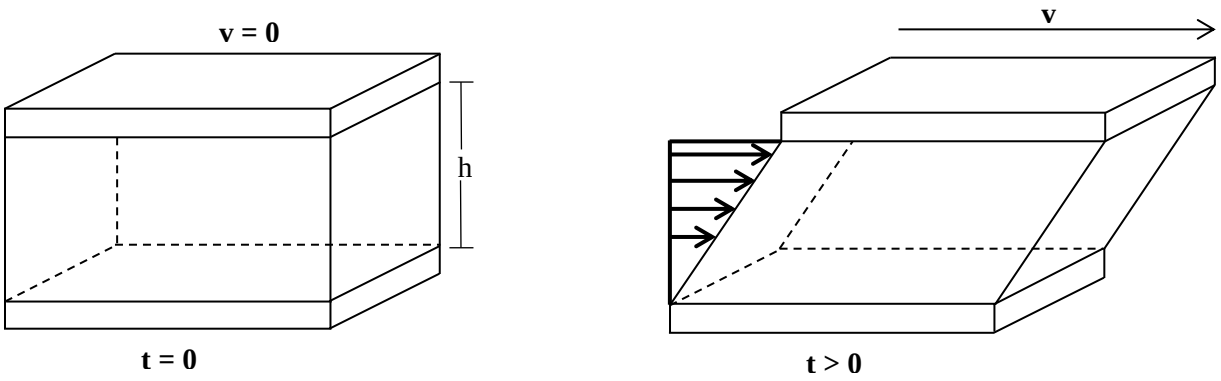

Figure 2.3 Schematic of steady shear flow

2.2.2 Sinusoidal Oscillation

The more generally used technique to determine the viscoelasticity of materials is the sinusoidal oscillation. Using this technique, two major rheological parameters are derived from the shifted stress wave equation: elastic modulus and viscous (loss) modulus. These rheological parameters provide insight into the flow property of structured fluids and the interrelation between the micro-structure of fluids and flow behavior.

Dynamic shear flow is characterized by the application of a sinusoidally varying motion (deformation) The flow is shown in Figure 2.4.

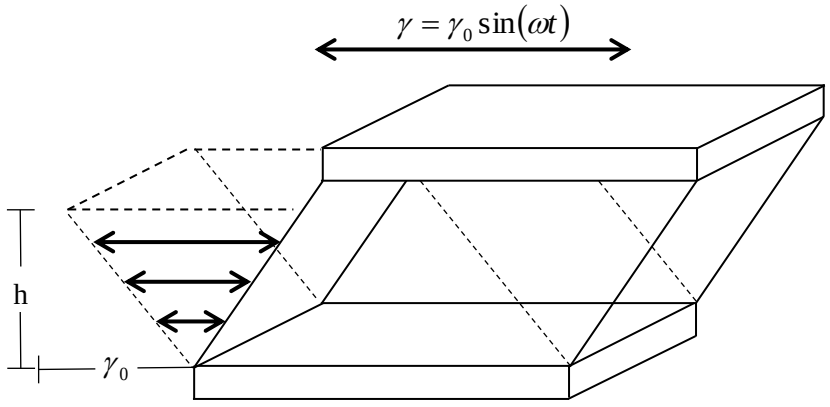

Figure 2.4 Schematic of oscillatory shear flow

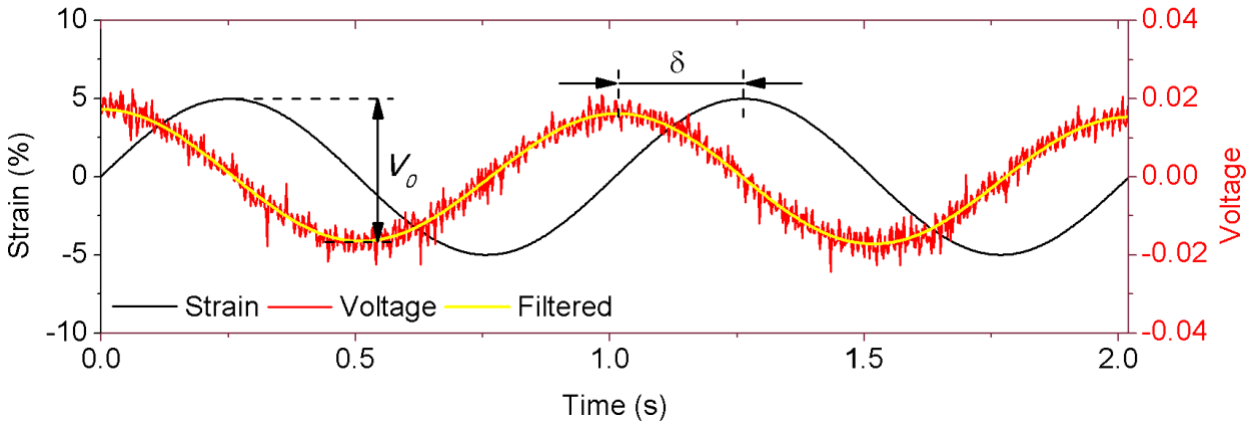

Figure 2.5 Strain and the resulting stress transducer signal in sinusoidal oscillation mode

In general, an oscillatory measurement is a technique that is useful to evaluate the viscoelastic properties of materials. Rheological parameters that can be evaluated from the oscillatory measurement include the complex modulus (G^*), storage modulus (G'), loss modulus (G''), and complex viscosity (η^*). When a sample is sheared sinusoidally at a certain amplitude of strain and frequency, the resulting shear stress also oscillates in response to the applied strain at the same frequency, but it is shifted by a certain phase angle depending on the material as shown in Figure 2.5. This is expressed as follows:

$$\gamma = \gamma_0 \sin \omega t \tag{2.11}$$

$$\tau = \tau_0 (\sin \omega t + \delta) \tag{2.12}$$

where γ_0 is the amplitude of the strain, τ_0 is the amplitude of the stress, ω is the angular frequency of the oscillation, and δ is the phase difference between the strain and stress wave. The value of the phase difference, δ, is 0 ° for an ideally elastic solid and 90 ° for an ideally viscous liquid, and it is often expressed in the form of tan δ, which is called loss tangent. The

phase shift of realistic materials falls between 0° and 90°. The stress, τ, can be broken into two sinusoidal waves: one is in phase and the other is out of phase by 90° with the strain wave.

$$\tau = \tau' + \tau'' = \tau_0' \sin \omega t + \tau_0'' \cos \omega t \tag{2.13}$$

Here, we can define two dynamic moduli: the storage modulus *G*', which represents the elastic portion of the complex shear modulus, and the loss modulus *G*'', which represents the viscous portion.

$$G' = \frac{\tau_0'}{\gamma_0} \tag{2.14}$$

$$G'' = \frac{\tau_0''}{\gamma_0} \tag{2.15}$$

Once the exact forms of the strain and stress are known, the rheological parameters can be easily calculated using the following equations:

$$\left|G^*\right| = \frac{\tau_0}{\gamma_0} \tag{2.16}$$

$$G' = \left|G^*\right| \cos\delta \tag{2.17}$$

$$G'' = \left|G^*\right| \sin\delta \tag{2.18}$$

$$\left|\eta^*\right| = \frac{\left|G^*\right|}{\omega} \tag{2.19}$$

2.3 Rheometers

A rheometer is an instrument used to characterize the rheology of a material. They are classified into two main categories depending on how the shear is induced: pressure-driven rheometers and drag flow rheometers.

2.3.1 Pressure-Driven Rheometers

Flow in pressure-driven rheometers is induced by a pressure difference along a hollow die where the pressure is generated by gravity or a piston. The types of pressure driven rheometers are defined by the geometry of the die; the most popular geometries are capillary (cylindrical) and slit die (thin rectangular slit). Both types of rheometers have been widely used to simulate processes such as polymer extrusion and pipeline transportation due to the similarity of the flow. The schematic of a typical capillary rheometer is shown in Figure 2.6 (a).

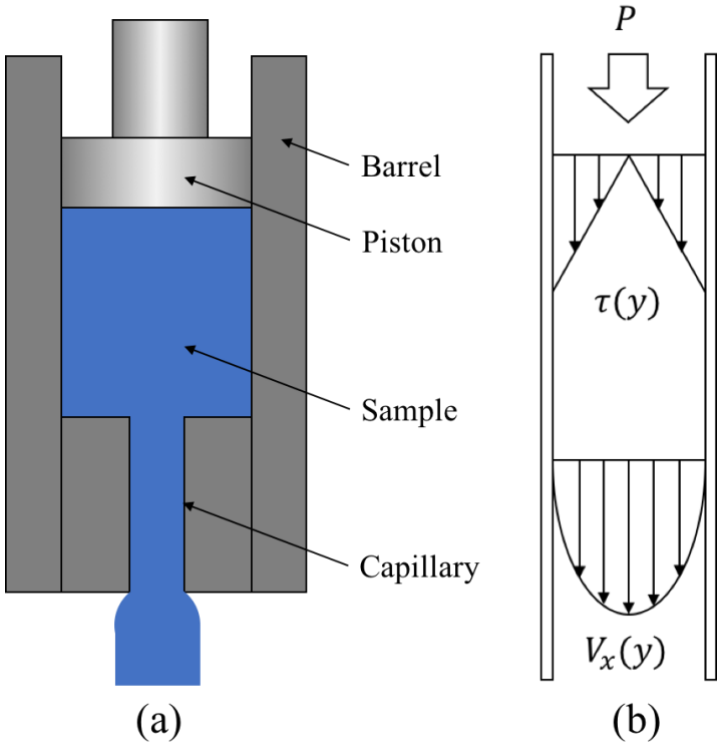

Figure 2.6 Schematic of a capillary rheometer (a) and the pressure and velocity profile in the barrel

Pressure drop and flow rate through the tube are measured variables in capillary rheometers. Shear stress cannot be directly calculated, but pressure drop and flow rate should be used with several assumptions to estimate the viscosity of fluids. The flow in the capillary is nonhomogeneous thereby causing non-uniform shear stress and strain rate. Figure 2.6 (b) shows the velocity profile in a capillary tube; shear rate is at a maximum at the wall and zero at the center. Shear stress and shear rate at the wall should be determined. Bagley end correction is often used to obtain shear stress on the wall (τ_w) and can be expressed as follows:

$$\tau_w = \frac{P_d}{2\left(L_0/R_c + e\right)} \tag{2.20}$$

where P_d is the pressure drop in the capillary, L_0 is the length of the capillary, R_c is the radius of the capillary, and e is the Bagley end correction (Bagley 1957). Shear rate on the wall ($\dot{\gamma}_w$) is often determined by the Weissenberg-Rabinowitch equation as follows:

$$\dot{\gamma}_\omega = \left(\frac{3+b}{4}\right)\dot{\gamma}_A \tag{2.21}$$

where

$$b \equiv \frac{d\left(\log \dot{\gamma}_A\right)}{d\left(\log \dot{\tau}_\omega\right)} \tag{2.22}$$

and $\dot{\gamma}_A$ is the apparent shear rate for a Newtonian fluid that can be expressed as follows:

$$\dot{\gamma}_A \equiv \left(\frac{4Q}{\pi R_c^{\,3}}\right) \tag{2.23}$$

where Q is the flow rate (Rabinowitsch 1929).

Capillary rheometers have numerous advantages over other type or rheometers. They are the most accurate rheometer for measuring viscosity when a very long capillary is used, and they are relatively inexpensive. The closed nature of the system and absence of any free surface

provides additional advantages including no solvent evaporation and no sample escaping from the system, which often causes serious measurement errors in rotational rheometers. Although the capillary rheometer is a good choice when used to evaluate steady shear rheological functions, it cannot be used to measure dynamic or transient viscoelastic functions.

2.3.2 Drag Flow Rheometers

In drag flow rheometers, a sample is placed between two geometries and the shear is induced by moving one geometry relative to another. The drag flow rheometers can operate either in strain controlled and stress controlled mode. Although there are numerous variations of drag flow rheometers, the most common types, falling ball, parallel plate, and rotational rheometers, are discussed here.

Falling ball rheometer

Falling ball rheometers measure the time required for a ball to fall a given distance in a fluid. Different shear rates can be applied by using balls with different diameters or densities, or by tilting the tube on an angle. However, these rheometers are rarely used for rheological studies because the flow field induced by the ball is extremely complex and requires a constitutive equation for complete analysis. Zero-shear viscosity is often reported because the flow is very slow. The zero-shear viscosity (η_z) is expressed as follows:

$$\eta_z = \frac{2(\rho_b - \rho_f)gR_b^2}{9v_\infty} \tag{2.24}$$

where ρ_b and ρ_f are the density of the ball and the fluid, respectively, g is the gravitational acceleration, R_b is the radius of the ball, and v_∞ is the terminal velocity. The schematic of a typical falling ball rheometer is shown in Figure 2.7.

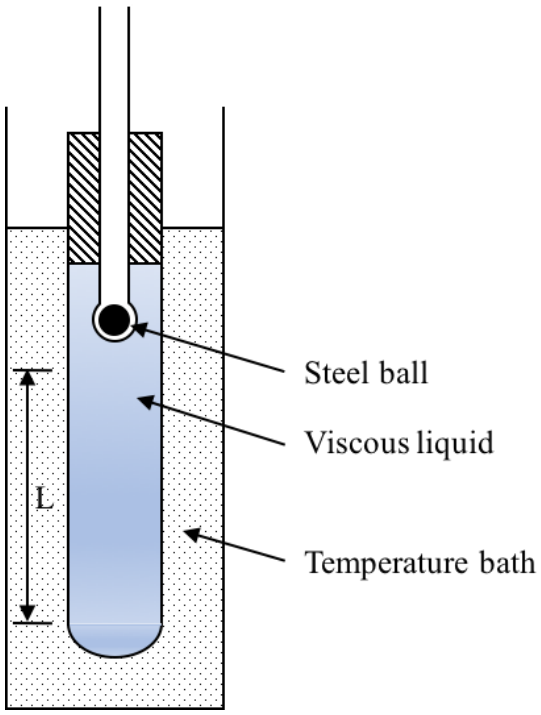

Figure 2.7 Schematic of a falling ball rheometer

Parallel plate rheometer

The parallel plate geometry is discussed in the previous chapter in the section that introduces the definitions of basic rheological quantities including shear stress, shear strain, strain rate, and viscosity. The shear flow that develops between the parallel plates is uniform throughout the sample if the flow near the edges of the plates is neglected. However, the edge effect becomes significant if the lengths of the edges are too small compared to the gap between plates. Another limitation of parallel plate rheometers is the difficulty in keeping the parallelism of the two plates for large strains and for large normal forces. Furthermore, the amplitude of strain is limited by the size of the plate thus steady shear measurements are impossible.

An attempt was made to mitigate the edge effect by developing a new rheometer. Giacomin et al. (1989) developed a sliding plate rheometer with a beam type shear stress transducer that was inserted into the middle of the plate to mitigate the edge effect.

Rotational rheometer

The most common type of rheometer is a rotational rheometer. In this configuration, a sample is placed between two plates that rotate in relation to one another. Typically, one rotates via electric motor, while the other plate serves as a torque transducer. Rotational rheometers are used to characterize a variety of materials with a wide range of viscosities.

Different head geometries may be used in a shear mode rheometer to better accommodate the material being tested. A few common head geometries are shown in Figure 2.8. The concentric cylinder, also called a Couette, shown in Figure 2.8(a), is commonly used for very low viscosity samples. This geometry is favorable because of its increased surface area compared to other available options. The cone and plate configuration, Figure 2.8(b), is the most common geometry used in rotational rheometers. This geometry provides the most consistent results and is a convenient method for obtaining true viscosity. Parallel plates, shown in Figure 2.8(c), are very similar to the cone and plate rheometer, except the flow between the parallel plates is not homogeneous, which makes the calculation slightly more complicated. In this study, concentric cylinder geometry was used for several reasons. First, since the focus in on the rheology of bitumen at higher temperatures where the viscosity is significantly reduced, the concentric cylinder would give more accurate measurements. Second, bitumen shows Newtonian behavior above certain temperatures, so it is not necessary to characterize non-Newtonian rheological properties such as normal force. Third, the concentric cylinder is much less sensitive to sample loading error.

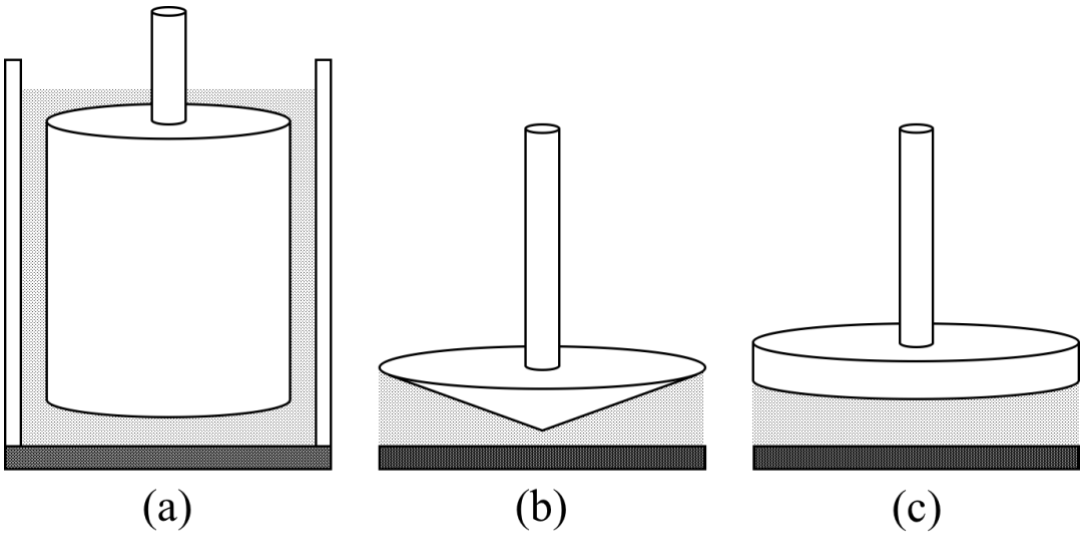

Figure 2.8. Three common head geometries for a rotational rheometer: (a) concentric cylinders, (b) cone and plate, and (c) parallel plates

In addition, torque measurement techniques are a primary measured variable in rotational rheometers, and the accurate measurement of torque is paramount for reliable rheological measurements. A torsion bar/spring has been widely used for torque measurements in rotational rheometers. The torsion bar/spring is attached to the inner or outer cylinder of the rotational rheometer and deflects to certain angle depending on the torque exerted on it. The amount of deflection is measured using a capacitance gage, linear variable differential transformer (LVDT), optical device, etc. The measurement range depends on the stiffness of the torsion bar/spring which means that an extremely small torque value can be accurately measured if a very thin torsion bar is used. However, the issue with using torsion bar/spring is that they have low resonant frequency, which reduces the range of transient or dynamic rheological measurements (Macosko 1996). Moreover, the deflection of the torsion bar/spring leads to significant errors in the strain or strain rate imposed on a fluid. Murata et al. (1987) developed a damped oscillation

rheometer consisting of a cylindrical tube suspended from a torsion wire that was filled with the liquid to be tested. Karmakar and Kushwaha (2007) developed a rheometer to determine soil visco-plastic parameters that work on the principle of torsional shear applied to a standard vane with controlled strain rate.

Another torque measurement technique is using a feedback control servo. This technique utilizes the motor drive current for torque measurements rather than using a separate torque measurement unit. With the recent advances in automation and control, this technique has become a popular way of measuring torque in rotational rheometers (Lauger 2008). It does not require deflection of the components to measure torque. Moreover, the stress control mode can be easily implemented with this method which enables the measurement of creep compliance and yield stress of a material. The torque range is only limited by the size of the servo motor that is being used. However, the response time of the servo system can cause delay and/or error in the torque measurement. Even very well-tuned servo system takes time to stabilize. In addition, the inertia of the shaft and spindle also causes erroneous measurement.

Considering the drawbacks associated with the current torque measurement techniques used in rotational rheometers, a more reliable and accurate torque measurement technique is needed. In this study, a piezoelectric torque transducer is used as an alternative method to measure torque in rotational rheometers. The benefits of piezoelectric torque transducers compared to the torsion bar/spring and the feedback control servo based torque transducers are their higher resonance frequency and negligible transducer inertia due to their high stiffness. Moreover, they have a high linearity over a wide range of torque values and are less sensitive to temperature.

2.3.3 High Pressure Rheometers

Various industrial processes involve the flow of fluids under high pressure conditions. Flow under high pressure is significantly different from the flow under ambient pressure and sometimes involves the dissolution of gas which cause further change the rheological response of a fluid.

High pressure rheometers are not significantly different from the above conventional rheometers. They are often modification of the conventional rheometers to accommodate high pressure in the system. High pressure in this context excludes hydraulic pressure, and only gas pressure rheometers are discussed here. A summary of high pressure rheometers is presented in Table 2.1.

Table 2.1 Summary of high pressure rheometers

Type	**Feature**	**Researchers**	**Year**	**P (MPa)**	**T_{max} (°C)**	$\dot{\gamma}(s^{-1})$
Falling ball	Magnetic force	Bae and Gulari	1997	5	Room T	N/A
Capillary		Gerhardt et al.	1996	N/A	N/A	N/A
Capillary	On-line	Lee and Park	1999	N/A	N/A	N/A
Rotational	Magnetic coupling	Oh et al.	2002	N/A	N/A	N/A
Rotational	Magnetic coupling	Khandare et al.	2000	7.6	500	100 – 250 rpm
Rotatioanl	Porous cup	Wingert et al.	2009	20	N/A	10^{-7} – 1200 rpm
MLSR	Magnetically levitated sphere	Royer et al.	2002	42	N/A	10^{-3} - 1

Falling ball rheometers can be easily modified for high pressure applications. Bae and Gulari (1997) developed a high pressure falling ball viscometer to measure the viscosity of PDMS-CO_2 systems at elevated pressures up to 5 MPa. The schematic of the falling ball

viscometer is shown in the Figure 2.9. An inherent problem of falling ball rheometers is that controlling the shear rate is difficult, because the shear rate is determined by the density and the viscosity of the fluid. Moreover, the shear rate must be in the range of the Newtonian plateau.

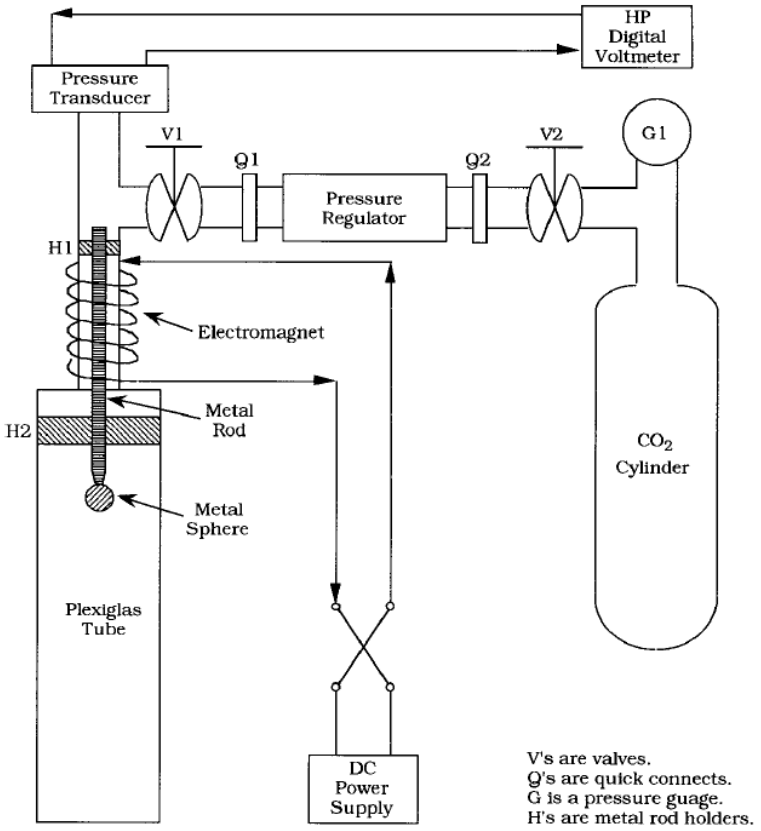

Figure 2.9 Schematic diagram of a falling-ball viscometer (Bae and Gulari 1997)

To overcome the drawbacks of conventional falling ball rheometers, Royer et al. (2002) developed a magnetically levitated sphere rheometer (MLSR). The basic design of the developed rheometer is very similar to a conventional falling ball rheometer as shown in Figure 2.10. In this design, ball is held at a fixed position using magnetic levitation, while the sample cylinder that contain the ball moves vertically using a motor to generate desired shear flow. Shear stress can

be calculated by measuring the magnetic force required to hold the ball. Therefore, some of the inherent limitations of falling ball rheometers can be eliminated.

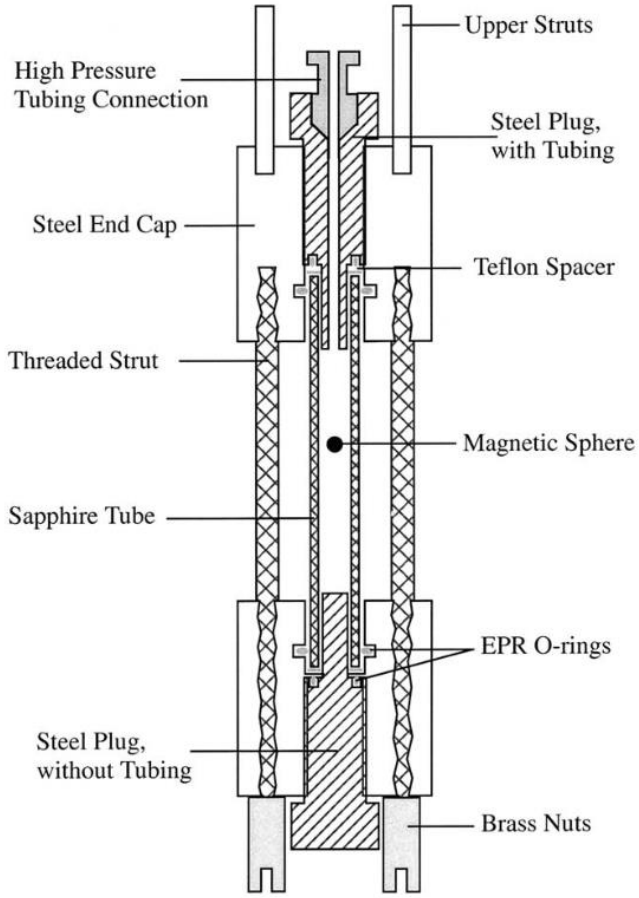

Figure 2.10 Schematic diagram of the high pressure chamber for the MLSR (Royer et al. 2002)

Capillary rheometers have been widely used for high pressure applications mostly by modifying existing designs. They also can be easily adopted for on-line measurements for die extrusion processes. Gerhardt et al. (1997) modified a commercial capillary extrusion rheometer. They added a back-pressure assembly, the main change, where the outlet pressure of the solution was kept constant above its bubbling point to prevent phase separation. The useful shear rate range reported was limited to 35 to 1500 s^{-1} due to plunger friction and difficulties in back

pressure control. Although the operating temperature and pressure limit was not reported in their work, temperatures of 50°C and 80°C and saturation pressures of 2.8 to 9.1 MPa were reported as the operating pressure of the PDMS-CO_2 system. A schematic of the capillary extrusion rheometer is shown in Figure 2.11.

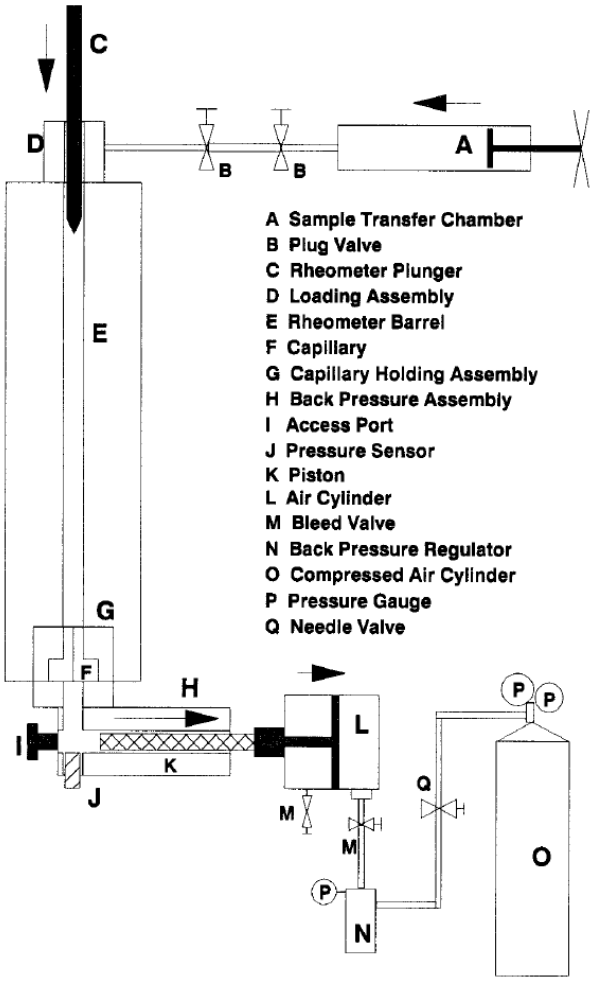

Figure 2.11 Schematic of a capillary extrusion rheometer (Gerhardt et al. 1997)

Lee et al. (1999) developed an on-line capillary rheometer attached to a foam extrusion line to determine the viscosities of a PS/supercritical CO_2 solution. The outlet pressure was regulated by a nozzle attached at the end of the capillary to prevent any phase separation due to

CO_2 precipitation. Pressure range was reported to be from 0.1 to 25 MPa, and the temperature range was not reported. A similar rheometer was developed by Areerat et al. (2002) and viscosities of LDPE/CO_2 at temperatures of 150°C and 175°C and CO_2 feeding pressures of 0 to 8 MPa were measured. One major problem associated with capillary rheometers is the large pressure drop across the capillary thus making it difficult to analyze the data corrected from the rheometer. Furthermore, it is difficult to change the shear rate and pressure independently because the shear rate is changed by adjusting the upstream pressure affecting the overall pressure profile. A schematic of the on-line capillary rheometer attached to an extruder is shown in Figure 2.12.

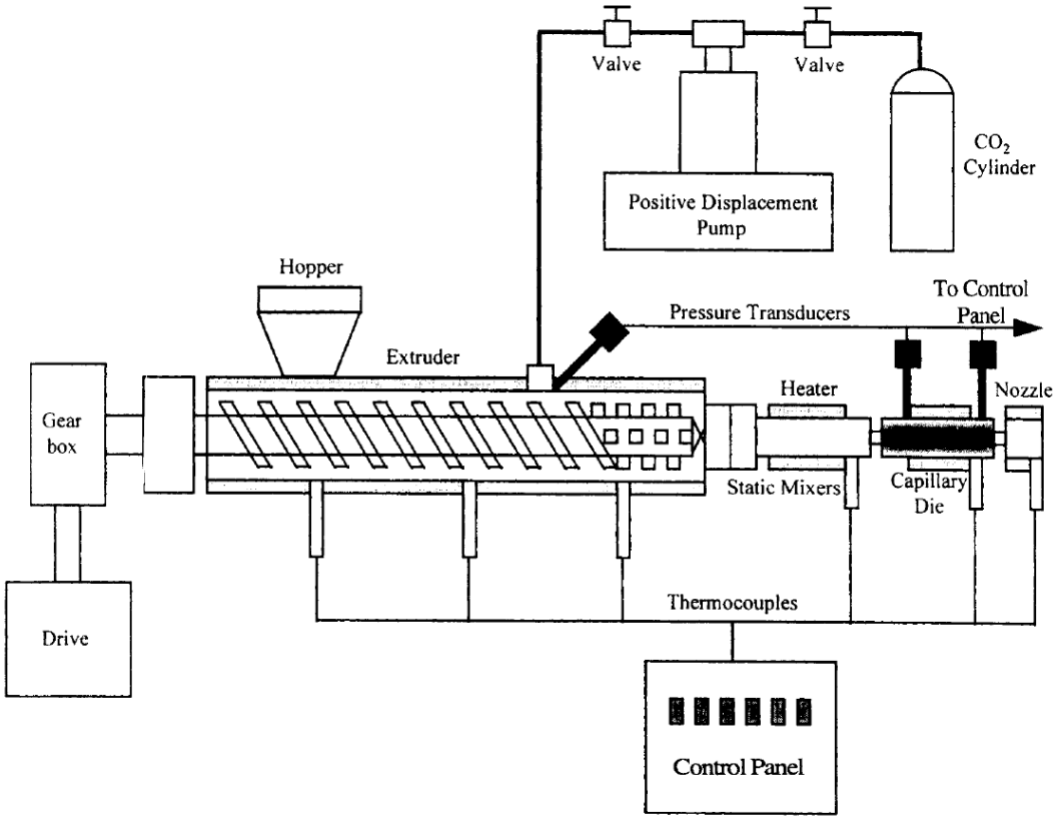

Figure 2.12 Schematic of an extruder with an on-line capillary rheometer (Lee et al. 1999)

This pressure gradient complexity can be eliminated using a rotational rheometer, which can operate under static and saturated pressure. One major advantage of using rotational rheometers is that they can be used to study the viscoelasticity of fluids. A high temperature, high pressure (HTHP) rotational rheometer was developed to measure the viscosities of pitch materials at elevated temperatures and pressures (Khandare et al. 2000a). A schematic of the HTHP rheometer is shown in Figure 2.13. The rheometer was a concentric cylinder type where the inner cylinder was driven by a DC motor, and the torque exerted on the outer cylinder was measured using a moment arm coupled with a linear variable differential transducer (LVDT). An oil bath was utilized to reduce vibration and oscillation on the moment arm. The concentric cylinder was built from a high pressure vessel with a magnetic coupling drive, which ensured leak-free rotational motion. The maximum operating pressure and temperature was 7.6 MPa and 500°C, respectively. (Khandare et al. 2000a) determined the upper and lower boundaries of the measurement range based on various factors including the magnetic drive torque limitation, mechanical torque limitation, and flow instability due to Taylor vortices. Considering these factors, the range of viscosity that could have been measured was between 10 and 500,000 mPa·s. They successfully measured the viscosity of carbonaceous pitch material at various temperatures and shear rates and validated the experimental results with commercial viscometers (Khandare et al. 2000b). Although they named it as a rheometer, the only rheological parameter reported was viscosity. This reason seemed to be attributed to the low compliance and rigidity of the moment arm, which was only suitable for steady shear measurements. Moreover, they did not present any high pressure rheological measurements using the developed rheometer.

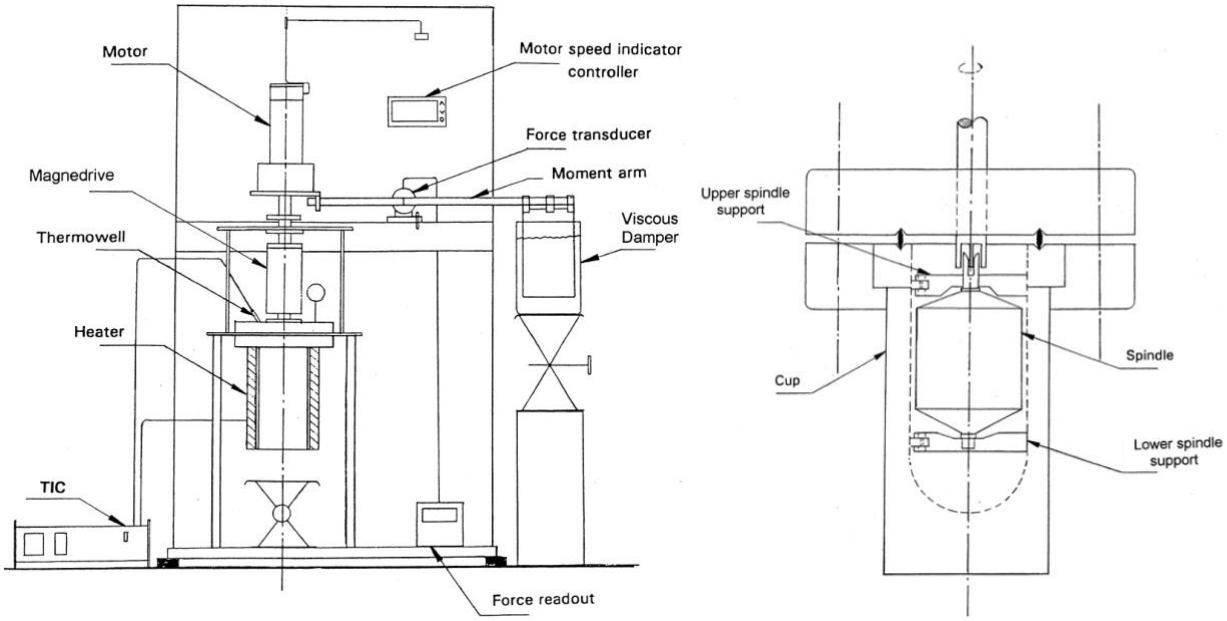

Figure 2.13 Schematic of (a) the high-temperature, high-pressure rheometer and (b) the cup-spindle assembly (Khandare et al. 2000a)

A high pressure rotational viscometer was developed by Oh and Lindt (2002). The developed viscometer was also a concentric cylinder type and relied on a magnetic transmission for transferring rotation to the inner cylinder. The viscosity of PS/CO_2 system was successfully measured in temperature ranging from 130°C to 200°C and under pressures up to 20.6 MPa. The viscometer operated in a relatively slow rate range between 0.01 and 1 s^{-1} (the Newtonian plateau region). However, they did not provide information on the torque sensor used.

2.4 Effects of Dissolved Gases on Rheology

Rheological properties of materials are affected by the dissolution of gases. Several theoretical and experimental studies have been conducted to understand this dependency, primarily in polymer processing. Theoretical models for the temperature, pressure, and dissolved

gas dependency that have been developed based on the free volume theory are discussed in this chapter.

2.4.1 Free Volume Theory

Doolittle's free volume theory (Doolittle 1951) described the effects of free volume on the viscosity of polymers. Doolittle's free volume equation is as follows:

$$\ln \eta = \ln A' + \frac{B'}{f} \tag{2.25}$$

where η is viscosity, f is the fractional free volume, and A' and B' are constants. Although it was originally developed to describe the temperature dependency on the viscosity of polymers, it has been found that the effect of other variables, such as pressure and diluent concentration, can be explained and described by the free volume concept.

2.4.2 Predictive Models Based on Free Volume Theory

Classical viscoelastic scaling methods, which employed a composition-dependent shift factor to scale both viscosity and shear rate, were used to reduce the viscosity data of the PDMS-CO_2 system to a master curve at each temperature (Gerhardt et al. 1997). Gerhardt et al. demonstrated that the main mechanism of the viscosity reduction upon the dissolution of gas involved both the dilution effect and an increase in free volume by comparing the PDMS-CO_2 system and the iso-free volume dilation.

The Kelly and Bueche equation was originally developed to express the viscosity of concentrated polymer solutions, based on Doolittle's free volume equation (Kelley and Bueche 1961). Gerhardt et al. (1998) modified this equation to describe the viscosities of PDMS-CO_2

systems. The concentration shift factor, a_c was explicitly expressed with fractional free volume as follows:

$$a_c = \frac{\eta_o(c)}{\eta_{o,p}} = (1 - w_c)^n \left[\frac{V_p}{V_m}\right]^n \exp\left[\frac{1}{f_m} - \frac{1}{f_p}\right] \tag{2.26}$$

where w_c is the weight fraction of dissolved CO_2, n is constant, V is the specific volume and f is the fractional free volume. Subscripts p and m denote the pure polymer melt and polymer-gas mixture, respectively. Fractional free volumes were estimated using two equation-of-state (EOS): Sanchez-Lacombe (S-L) and Panayiotou-Vera (P-V) equations as described in Garg et al. (1994). The S-L and P-V EOS are given by the following:

$$\frac{\tilde{P}}{\tilde{T}} = -\ln(1-\tilde{\rho}) - \left(1 - \frac{1}{r}\right)\tilde{\rho} - \frac{\tilde{p}^2}{\tilde{T}} \tag{2.27}$$

$$\frac{\tilde{P}}{\tilde{T}} = \ln\left(\frac{\tilde{v}}{\tilde{v}-1}\right) + \frac{Z}{2}\ln\left(\frac{\tilde{v}+q/r-1}{\tilde{v}}\right) - \frac{\theta^2}{\tilde{T}} \tag{2.28}$$

where $\tilde{P}$, $\tilde{T}$, $\tilde{\rho}$, and $\tilde{v}$ are reduced pressure, temperature, density, and volume, respectively, r is the number of lattice sites occupied by a polymer chain, Z is the coordination number of the lattice, and q is the effective polymer chain length. This approach enabled the prediction of the viscosity of a polymer-gas system from the viscosity of a pure polymer melt without any rheological information of the polymer melt and gas. However, some thermodynamic parameters for mixed systems, such as the solubility of a gas, was required to complete the EOS characterization.

Lee et al. (1999) developed a generalized Arrhenius equation based on Doolittle's equation to express the viscosity of polystyrene(PS)/CO_2 as a function of temperature, pressure, and CO_2 concentration. The fractional free volume in Doolittle's equation is mathematically

expressed as a power law series by taking only the first order term. Then, the zero-shear viscosity (η_z) is expressed as a function of temperature (T), pressure (P), and CO_2 concentration (w_c) as follows:

$$\eta_z \approx A\exp\left(\frac{\alpha}{T-T_r}+\beta P+\psi w_c+constant\right)= \\ =A\exp\left(\frac{\alpha}{T-T_r}+\beta P+\psi w_c\right). \tag{2.29}$$

where A, T_r, α, β, and ψ are the unique constants for the polymer and gas that need to be determined experimentally. In addition to the generalized Arrhenius equation, a generalized Cross-Carreau equation was used to incorporate the shear thinning behavior of the PS/CO_2 system. Although the proposed model agreed well with the experimental data, the effect of pressure was not straight forward due to the pressure drop along the capillary.

Royer et al. (2000) took a different approach to calculate the free volume in Doolittle's equation. The William-Landel-Ferry (WLF) equation, which was an expression of the free volume as a function of temperature, was adopted along with the glass transition temperature depression model proposed by Chow. Pressure and concentration shift factors (a_p and a_c) were derived as follows:

$$
\begin{aligned}
\log(a_p) &= \log\left(\frac{\eta_{T,P,c}}{\eta_{Tg,mix,P,c}} \bullet \frac{\eta_{Tg,mix,Po,c}}{\eta_{T,Po,c}}\right) = \log\left(\frac{\eta_{T,P,c}}{\eta_{T,Po,c}}\right) \\
&= \frac{c_1\left(T - T_{g,mix,Po}\right)}{c_2 + T - T_{g,mix,Po}} - \frac{c_1\left(T - T_{g,mix,P}\right)}{c_2 + T - T_{g,mix,P}} \\
\log(a_c) &= \log\left(\frac{\eta_{T,Po,co}}{\eta_{Tg,mix,Po,c_o}} \bullet \frac{\eta_{Tg,Po,c}}{\eta_{T,Po,c}}\right) = \log\left(\frac{\eta_{T,Po,co}}{\eta_{T,Po,c}}\right) \\
&= \frac{c_1\left(T - T_{g,Po}\right)}{c_2 + T - T_{g,Po}} - \frac{c_1\left(T - T_{g,mix,Po}\right)}{c_2 + T - T_{g,mix,Po}}
\end{aligned}
\tag{2.30}
$$

where the subscripts P and P_0 refer to the viscosity data at a given pressure, P, and that are corrected to atmospheric pressure; and c and c_o refer to the CO_2 data and corrected to a CO_2 concentration of zero. The advantage of the proposed model is that it does not require P-V-T type data, which is often difficult to obtain experimentally, for the calculation. Rather the model requires the material parameters of polymers, which are available in the literature or can be obtained experimentally without much difficulty.

Since the linear temperature dependency of the WLF model is valid for temperatures only up to T_g + 100°C, the Arrhenius equation is used for temperatures above T_g + 100°C (Royer and DeSimone 2001). The pressure and concentration scaling factors (a_P and a_C) obtained using this approach as follows:

$$
\begin{aligned}
\ln a_P &= \ln\left(\frac{\eta_{T_{g,\,Po,\,mix}}}{\eta_{T_{g,\,P,\,mix}}}\right) = \left[\frac{E_a}{R}\left(\frac{1}{T_{g,\,Po,\,mix}} - \frac{1}{T_{g,\,P,\,mix}}\right)\right] \\
\ln a_C &= \ln\left(\frac{\eta_{T_{g,\,Po,\,mix}}}{\eta_{T_{g,\,Po}}}\right) = \left[\frac{E_a}{R}\left(\frac{1}{T_{g,\,Po}} - \frac{1}{T_{g,\,Po,\,mix}}\right)\right]
\end{aligned}
\tag{2.31}
$$

where E_a is the activation energy of pure polymers that should be obtained from viscosities.

Most of the predictive models discussed in this section are based on the free volume

theory. The problem associated with this theory is that it requires information on the volumetric parameters and thermodynamic properties of the gas, polymer, and mixture, and these parameters and properties are difficult to measure. Therefore, a predictive model that is easily applicable to polymer-gas systems is required. In this thesis, the generalized Arrhenius equation used by Lee et al. is modified and used to predict the viscosity of a PDMS-CO_2 system. The concentration of CO_2 in equation (2.29) is expressed as a function of temperature and pressure, so the viscosity can also be expressed as a function of temperature and pressure without the need for difficult thermodynamic calculations.

2.5 Summary

This chapter presented the theoretical background on rheology and viscoelasticity, various types of rheometers with their pros and cons, and high pressure rheometers that were developed to investigate polymer-gas rheology. A literature review of experimental and theoretical studies on polymer-gas rheology was also presented.

Pressure driven rheometers have been extensively used in polymer processing and pipeline engineering because of the similarity in the flow. However, the large pressure drop across the capillary or slit die limits the amount of gas dissolved in the fluid and causes non-uniformity within the sample. Falling ball rheometers also have also been widely used for high pressure rheological measurements due to their simple design and ease of operation. However, the shear flow induced by the ball is highly complex and difficult to analyze. Rotational rheometers can eliminate the problems related to pressure gradients and non-homogeneity because constant pressure throughout the sample can be achieved. Moreover, various rheological parameters can be measured using rotational rheometers.

Although several other studies have also developed rheometers, most of these rheometers have been torsion-based rather than torque-based. Even relatively stiff torsion bars must twist a little to record the torque, which can lead to significant errors in the strain or transient strain rate imposed on a sample. Therefore, in this study, a piezoelectric torque transducer, which is more rigid and thus has a higher resonant frequency, resulting in more accurate measurements, is used for torque measurement. Furthermore, the developed rheometer can determine not only viscosity, but also a wide range of other rheological properties, including G' (the storage modulus) and G'' (the loss modulus).

CHAPTER 3: EXPERIMENTAL SETUP

In this chapter, the design and implementation of the high pressure rotational rheometer is discussed. The novel design features of the developed rheometer are the utilization of a piezoelectric torque dynamometer and a high pressure dynamic seal both of which enable dynamic rheological measurements under pressurized gases. The overview of the design and the core components, including the piezoelectric torque dynamometer and charge amplifier, band heater and temperature controller, servo motor and motion controller, and bearing and dynamic seal, are discussed. Then, the materials (calibration fluid, PDMS, and CO_2) used for the rheological measurements are presented. The effect of the bottom plate gap is investigated to find the optimum gap where the end effect becomes negligible. Finally, the overall system is calibrated using the calibration fluid, and the methods for compensating and/or mitigating friction of the dynamic seal are presented.

3.1 Design of Rotational Rheometer

3.1.1 Overall Design

The developed rheometer is a rotational rheometer with concentric cylinders that shears a sample between the inner (i.e., bob) and the outer (i.e., cup) cylinder. Concentric cylinder geometry was chosen over other possible options because it is less sensitive to the sample volume, and therefore, it is less effected by sample loading errors and swelling due to the dissolution of gas. Further, concentric cylinder geometry makes more contact with a sample compared to the cone and plate and parallel plates geometry resulting in much higher torque imposed on a sample and more accurate rheological measurements.

The experimental setup and schematic of the developed rheometer are illustrated in Figure 3.17 and Figure 3.18. The rheometer is primarily a custom-designed vessel of ~50 mL capacity with a mechanical agitator mounted on a highly sensitive piezoelectric torque dynamometer. The mechanical agitator consists of a brushless DC motor, rotating shaft, and a cylindrical geometry that is attached to the end of the shaft. The motor is coupled with a differential encoder to track the exact position and velocity of the shaft. A single-axis motion controller with a software package provided by the manufacturer enabled the motor to operate in the desired manner. The dynamic seal used for the rotating shaft is a polytetrafluoroethylene (PTFE) lip seal with a stainless-steel U-spring. The vessel is also equipped with a gas inlet and outlet, a pressure gauge, and a rupture disc with a 700 psi pressure rating for high pressure experiments. The reactor is heated using a band heater, and the temperature is controlled using a benchtop temperature controller (Omega CSi32) coupled with a K-type thermocouple attached to the outer wall of the reactor. When the fluid inside the reactor is sheared by a rotation of the rotor, torque is exerted to the inner wall of the reactor depending on the rheological response of the fluid. This torque is measured at the piezoelectric torque dynamometer.

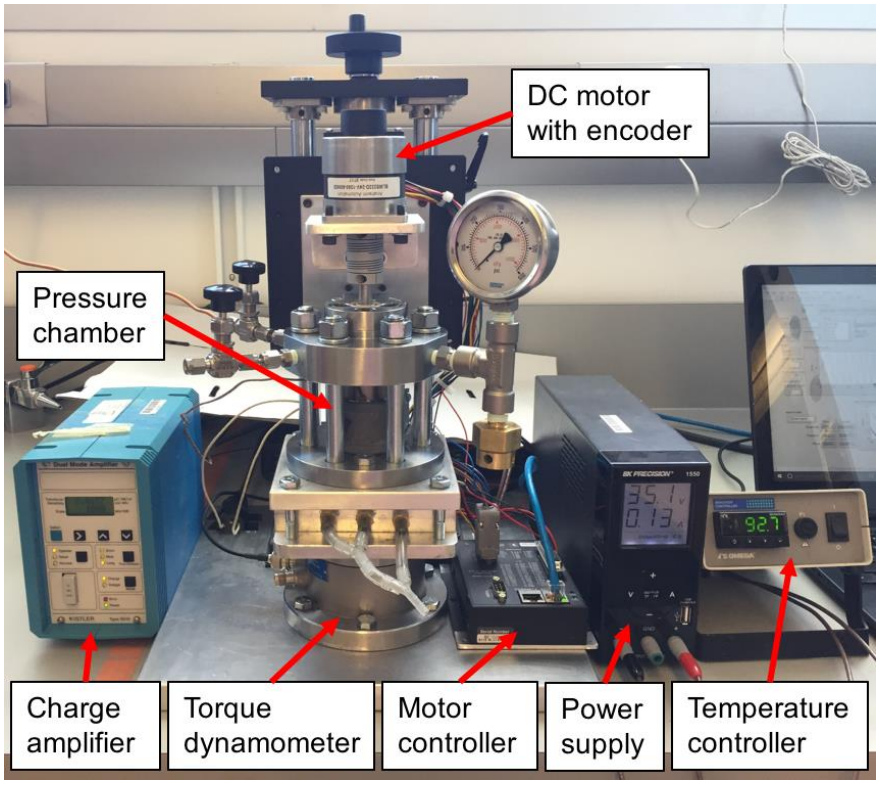

Figure 3.17 Picture of the assembled rheometer

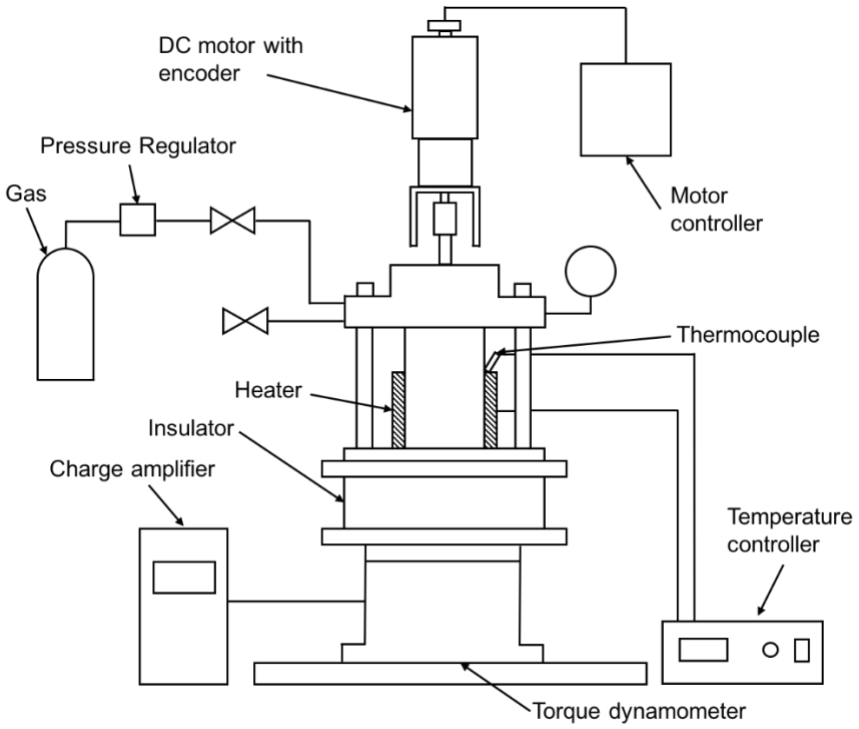

Figure 3.18 Schematic of the rheometer setup

3.1.2 Piezoelectric Torque Dynamometer

The torque transducer used in this study has built-in quartz measuring cells that have a piezoelectric property whereby electrical charges are generated in response to applied torque. The electrical charge is then amplified and converted to a voltage signal in a charge amplifier (Type 5010, Kistler).

The torque dynamometer is calibrated using a hammer instrumented with a force sensor. An aluminum bar with a length of approximately 25 cm is attached to the torque dynamometer and hit with a hammer at a distance of 10, 15, and 20 cm from the center of the torque dynamometer. The resulting torque, *M*, is calculated as follows:

$$M = dF \tag{3.1}$$

where *d* is the distance from the center of the torque dynamometer to the impact point, and *F* is the force measured by the hammer. As expected, the calculated torque was exactly proportional to the electrical signal from the torque dynamometer. Based on the calibration result, the transducer sensitivity and scale factor were determined and then entered into the charge amplifier, so that the voltage output from the charge amplifier became the actual torque value. The charge amplifier factors are shown in Table 3.5.

Table 3.5 Charge amplifier factors

Transducer Sensitivity (pC/N·m)	**Scale (N·m /Volt)**
0.0157	10000

Piezoelectric transducers have several advantages including a wide torque range, high linearity, and no hysteresis. Moreover, even an extremely small dynamic change in torque can be detected if the amplifier factor is adjusted. In fact, the quartz itself has an infinite resolution.

Therefore, the resolution of the torque dynamometer is only limited by the noise of the signal from the charge amplifier and the mechanical assembly of the rheometer. The technical specifications of the torque dynamometer are listed in Table 3.6.

Table 3.6 Technical specifications of the torque dynamometer

Range (N·m)	± 100
Threshold (N·cm)	~0.02
Linearity (%FSO)	≤ ±1
Hysteresis (%FSO)	≤ 0.5
Rigidity (N·cm/μrad)	50
Natural frequency (kHz)	> 3
Operating temperature range (°C)	0 – 70
Temperature coefficient of sensitivity (%/°C)	-0.02

It should be noted that the operating temperature range was between 0 and 70°C. An aluminum block with water cooling channels was placed between the torque dynamometer and the pressure cell. The water cooling system was used for rheological experiments that operated at temperatures higher than 150°C.

3.1.3 Temperature Control

As the rheological properties of materials are highly dependent on temperature, precise temperature control is essential to operate rheometers. A ceramic band heater coupled with a type-K thermocouple and a temperature controller is used with the rheometer in this experiment. Compared to other heating methods, using a band heater is easier to install and heats faster.

Thermal grease is applied between the band heater and the reactor wall to minimize heat loss and thermal gradient of the sample.

Fluid temperature was not directly measured from the inside of the reactor during the rheological measurements because the presence of a thermocouple might have affected the flow of the fluid under shearing. Therefore, it was necessary to estimate the temperature of the fluid from the temperature of the outer wall of the reactor. The temperature set-point was increased in 25°C increments from 50°C up to 150°C, and the corresponding fluid temperature was measured. A sufficient amount of time was taken until no change in temperature was observed to ensure thermal equilibrium of the system. It was assumed that there was no thermal gradient within the sample. The correlation between the temperature set-point T_{sp} and the fluid temperature T_{fluid} is plotted in Figure 3.19. Linear fitting of the data set resulted in the following correlation:

$$T_{fluid} = 0.79T_{sp} + 5.79 \tag{3.2}$$

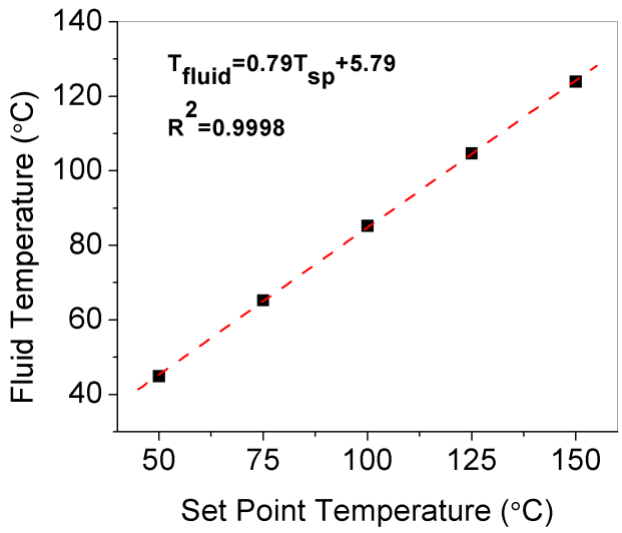

Figure 3.19 Temperature set point vs. fluid temperature

3.1.4 Motion Control and Data Acquisition

Another main component of the developed rheometer is a motor and motion controller. A brushless DC motor was chosen in this study due to its advantages compared to a brushed DC motor and a stepper motor: (1) smooth motion that minimizes system vibration and noise, (2) excellent dynamic response, (3) higher speed, (4) higher torque than a comparably sized brushed motor, and (5) a lower cost of maintenance. The technical specifications of the motor are listed in Table 3.3. A quadrature encoder was assembled on the motor for keeping track of the position and speed of the motor shaft. The resolution of the encoder was 20,000 PPR (pulses per revolution), which corresponded to 0.018 degrees. The motor and encoder were connected to a single-axis motion controller (DMC-31012, Galil), which controlled the motor using a closed loop feedback. The motion controller had a built-in amplifier and communicated with a PC via Ethernet.

Table 3.3 Technical specifications of the brushless DC motor

Rated voltage (V)	24
Rated power (W)	16
Rated speed (rpm)	1350
Rated torque (mN·m)	110.0
Torque constant (mN·m/A)	116.0

PID tuning parameters were determined to minimize the error between the commanded and the actual motion profile. It should be noted that the tuning parameters were different depending on the profile of motion and the load (friction and/or torque) acting on the shaft of the motor. In certain conditions, the motion profile was highly sensitive to the tuning parameters and

did not follow the exact profile of the commanded motion. Therefore, the motion profile should always be monitored to ensure whether it follows the commanded profile.

The motor controller also had many input and output ports for analog and digital signals and a non-volatile memory that could record data in an array of up to 3000 elements (maximum 6 arrays) every 1 mins. Therefore, both the encoder and the torque signals could be recorded without using a separate data acquisition board. Computer programs were developed using LabVIEW for the motion control, monitoring/recording the analog and digital outputs, and calculating the rheological parameters. The schematic diagram of the motion control and torque measurement components and their connections are shown in Figure 3.20.

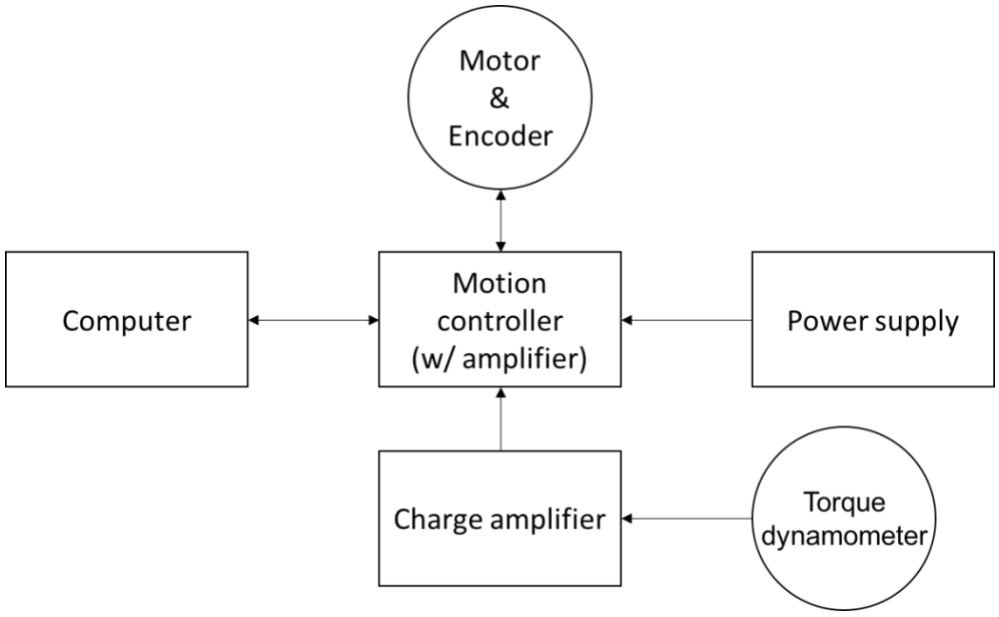

Figure 3.20 Elements of motion control and torque measurement

3.1.5 Bearing and Dynamic Seal

The rheometer utilizes a high temperature plastic ball bearing with stainless steel balls for precise concentric rotational motion of the rotor with minimum friction. The dynamic seal used

to rotate the shaft is a PTFE lip seal with a stainless-steel U-spring. It has a continuous operating pressure of 20.7 MPa and a temperature of 200°C, which are much higher values than the operational range investigated in this study. The self-lubricating property of the seal allows for use in dry conditions while maintaining pressure in the chamber even at rotational speeds up to 12,223 rpm (1,200 fpm). It should be noted that a slight leak occurred at the dynamic seal when the vessel was pressurized. For this reason, gas was constantly fed into the vessel to maintain the pressure. Further, there was a slight eccentricity due to the dimensional inaccuracy of the machined parts and the bearing clearance.

A high pressure rotational rheometer was assembled using the components discussed above. The function of the individual components along with their capabilities and limitations are discussed in this section. In the following sections, the optimization and calibration of the overall system is discussed.

3.2 Materials Studied

A certified Newtonian calibration fluid (Brookfield, #CAP8L) with a viscosity of 5,237 mPa·s (at 25°C) was used in this study to calibrate the overall system and some preliminary rheological measurements.

The investigated materials in this study are PDMS and CO_2. The PDMS used in this study is PSF-12500cSt from Clearco Products Co., Inc. It has a kinematic viscosity of 12,500 cSt and a density of 0.97 g/cm^3 at 25°C. From the silicone fluid equivalents chart provided by the manufacturer and from information in an earlier study, PDMS is expected to have a molecular weight (M_w) of 95,000 g/mol (Royer et al. 1999). CO_2 with a purity of 99.9 % was purchased from Praxair Co., Canada.

PDMS is chosen instead of heavy oil to avoid experimental difficulties and uncertainties that can result from using heavy oil. Rheological measurements using heavy oil can be significantly affected by the evaporation of lighter hydrocarbons, thermal degradation, phase separation, etc. PDMS is the simplest silicone that has a silicone-oxygen-silicone backbone, which is the basic structure of silicones. Another reason for choosing PDMS is for safety; it does not produce any toxic gas and non-flammable. PDMS is a good model polymer melt to investigate the gas plasticization of polymer melts due to its high gas solubility mostly with CO_2. The low melting temperature of PDMS eliminates the experimental difficulty of melting engineering thermoplastics.

3.3 Gap Optimization

In concentric cylinder geometry, it is assumed that torque induced on the outer cylinder is mostly due to the shearing of the fluid between the inner and outer cylinder. However, there is an extra torque contribution due to the shearing of the fluid between the bottoms of the cylinders, which is commonly referred to as "end effect." This effect is one of the major sources of error in concentric cylinder rheometers and should be minimized or corrected. In this section, the effect of the bottom plate gap is evaluated using the Newtonian calibration fluid at various gap distances. The gap distance that is used for the subsequent rheological measurement is determined based on the result.

The torque of flow at the bottom of the cylinder can be approximated as a flow between parallel plates. The extra torque contribution at the bottom of the cylinder can be estimated using the following equation:

$$M_p = \frac{\pi R_i^4 \eta \Omega}{2h} \tag{3.3}$$

where R_i is the radius of the inner cylinder, η is the viscosity of a Newtonian fluid, Ω is the angular velocity, and h is the distance between the plates. The torque contribution at the wall of cylinder can be expressed as follows:

$$M_c = \frac{-4\pi R_o L \eta \Omega}{1-(R_i / R_o)^{-2}} \tag{3.4}$$

where R_o is the radius of the outer cylinder, L is the length of the cylinder. Therefore, the total torque can be expressed as the sum of these two contributions:

$$M_{tot} = M_c + M_p \tag{3.5}$$

Figure 3.21 shows the theoretical estimation and experimental measurement of the total torque as a function of the gap spacing at the bottoms of the cylinders at various angular velocities using the calibration fluid. Since M_p is inversely proportional to h, the torque contribution at the end of the cylinder could be negligible if h is large enough compared to the gap between the concentric cylinders ($R_o - R_i$). According to the theoretical calculation, the torque contribution due to the end effect at a 3.2 mm gap was only 5.4 % of M_c. Experimentally, a parallel gap larger than 3.2 mm has a negligible contribution on the total torque measurement. Therefore, the gap spacing was fixed at 3.2 mm for all experiments conducted in this study.

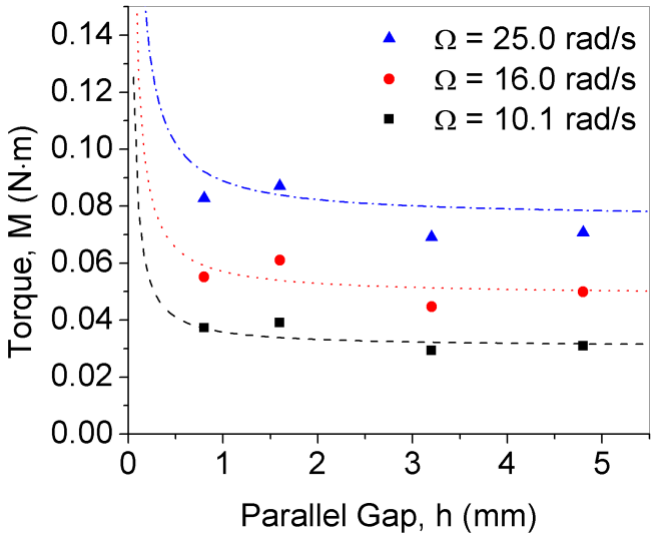

Figure 3.21 Theoretical estimation compared with experimental data of the total torque values versus the distance of the parallel gap

3.4 Rheometer Calibration

The calibration of the overall system includes compensation for system friction and the evaluation of the calibration coefficient. The methods used for the friction compensation are discussed along with their limitations. Then, the calibration coefficient is determined using a calibration fluid with known viscosity.

3.4.1 Friction Compensation

The developed rheometer utilizes a high pressure dynamic seal, which produces additional torque due to the friction between the seal and the shaft. This torque is quite high compared to the torque caused by the shearing of the test fluid. Therefore, the torque measurement should be compensated for the friction. The measured torque $M_{measured}$ is the sum of the two contributions:

$$M_{measured} = M_{fluid} + M_{friction} \tag{3.6}$$

where M_{fluid} is the torque cause by the shearing of the fluid, and $M_{friction}$ is the torque caused by the friction between the seal and the shaft. The torque caused by the seal friction should be subtracted from the measured torque to obtain the torque caused by the shearing of the fluid.

The seal friction under steady shear mode was evaluated by rotating the rheometer without any liquid at various rotational speeds and measuring the resulting torque. All measurements were repeated three times. Shear rates were calculated using the angular speed and geometry of the concentric cylinder:

$$\dot{\gamma} = \frac{-2\Omega}{1-\left(\frac{R_i}{R_o}\right)^{-2}} \tag{3.7}$$

The torque values measured while the empty rheometer was rotated at various shear rates are shown in Figure 3.22. The torque was 0.093 N·m at 15.6 s^{-1}; it increased to 0.116 N·m as the shear rate increased. These values are significant considering the torque exerted on the fluid (the maximum torque that the motor can produce is approximately 0.25 N·m). The large friction value can result in a large measurement scatter, especially at lower shear rates.

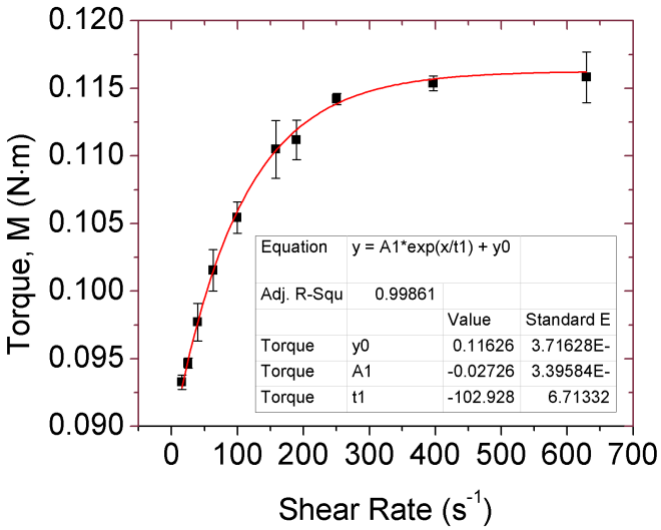

Figure 3.22 Torque as a function of shear rate due to system friction

The large friction of the seal was mitigated by pre-shearing. In other words, the rheometer was rotated at a very low speed (10 rpm) at the beginning and was subsequently increased to a desired speed. The resulting torque (0.002 – 0.026 N·m) and the measurement scatter were much smaller after pre-shearing. The measured friction is shown in Figure 3.23. The red line indicates an exponential fit, which is given by the following:

$$M_{friction} = 0.02788 - 0.0176\exp(\frac{-\dot{\gamma}}{59.6396}) - 0.01316\exp(\frac{-\dot{\gamma}}{305.9678}) \qquad (3.8)$$

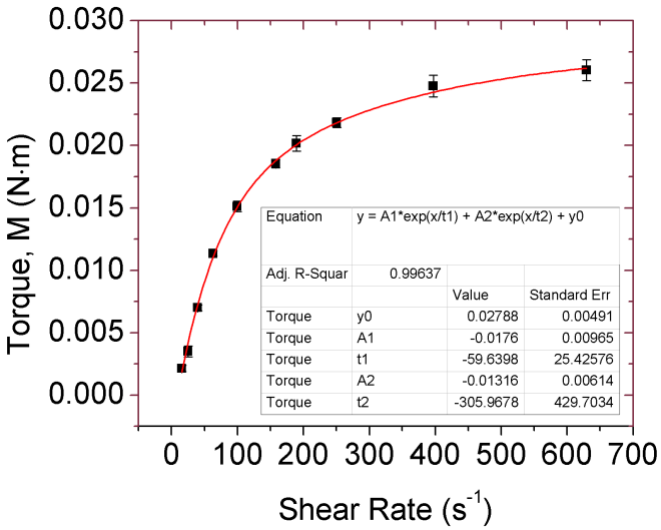

Figure 3.23 Torque as a function of shear rate due to system friction

If a fluid is measured in the same manner (pre-shearing) and the torque given by the above equation is subtracted from the total torque, the torque from the shearing of the fluid can be easily determined. However, the torque (or shear stress) curve does not pass through the origin anymore because the torque contribution is missing between 0 – 10 rpm (Figure 3.24). This issue could be corrected by vertically shifting the curve so that the curve passes through the origin, assuming that the torque and shear rate is linear between 0 – 10 rpm. This approach is reasonable because many fluids, including polymeric liquids, have a Newtonian plateau region where the shear stress and the shear rate have a linear relationship at low shear rates. Since PDMS also has a distinctive Newtonian plateau, it is not problematic to correct the torque and to get reliable, steady shear results. However, some fluids that have non-linearity at low shear rates or yield stress cannot be corrected in this way.

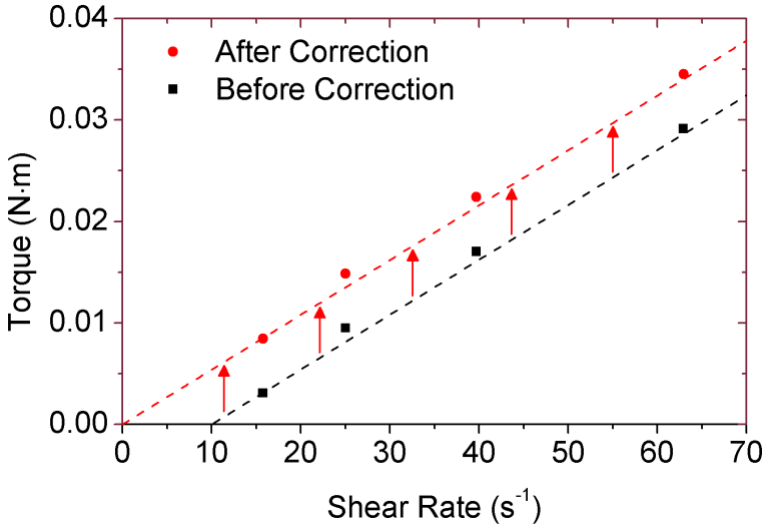

Figure 3.24 Torque correction scheme in steady shear mode

In the sinusoidal oscillation mode, it is difficult to evaluate the friction because the shear rate changes continuously over time. The blue line in Figure 3.25 is the torque that is measured in the sinusoidal oscillation mode without any fluid present in the rheometer. The torque profile was periodically repeated at the same frequency with the strain. A drastic change in torque was observed near the points where the strain rate reached zero (i.e., where the rotational direction changed). After the drastic change in torque, a small bump was observed, and a region developed where the torque remained relatively constant. This complex torque profile is due to the complexity of the friction phenomena, and there are several theories and predictive models for these phenomena. For example, the small bump after the drastic change in torque can be explained by the Stribeck effect (Jacobson 2003). However, this phenomenon is only valid for steady-state friction; dynamic friction poses additional complexities for estimating the friction. To avoid these complexities, the frictional torque signal is recorded for every combination of strain amplitude and frequency used in the sinusoidal oscillation measurement, and it is subtracted from the torque signal when the fluid is present. The phases of the two signals are

matched before the subtraction. The torque signal after the subtraction shows a smooth sinusoidal profile with minimal distortion as shown in Figure 3.25.

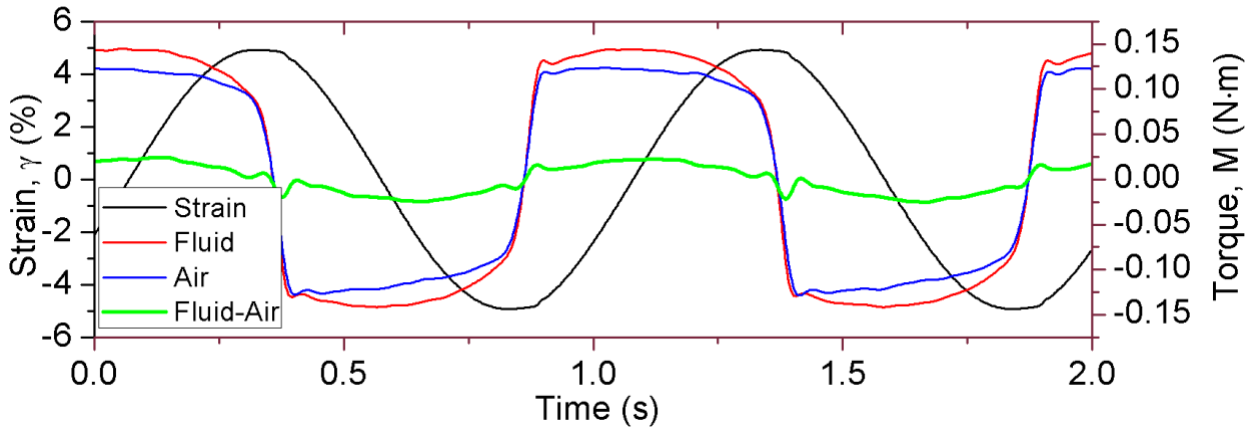

Figure 3.25 Torque correction scheme in sinusoidal oscillation mode

3.4.2 Calibration

The primary measured variable in the rotational rheometer is torque. This primary measured variable should be converted to corresponding shear stress to calculate the rheological parameters. Theoretically, shear stress acting on the outer cup of the rheometer is given by the following equation:

$$\tau = \frac{M_o}{2\pi R_o^2 L} \tag{3.9}$$

where M_0 is the torque measured on the outer cylinder. However, in reality, it is not only the shearing of the fluid on the wall of the cylinder that affects the torque measurement. There is a variety of other uncertainties that contribute to the torque measurement, such as dimensional error, eccentricity, end effect, and wall slip. Therefore, the calibration coefficient should be obtained to find the exact correlation between the measured torque and corresponding shear stress. A calibration fluid with a viscosity of 5,237 mPa·s was tested in steady shear mode using

shear rates ranging from 17.7 to 237.9 s^{-1}. Shear stress τ can be easily calculated from the definition of shear viscosity as follows:

$$\tau = \eta\dot{\gamma} \tag{3.10}$$

The calibration result is shown in Figure 3.26. The measured torque and calculated shear stress were exactly proportional, and the calibration coefficient was 12,583 m^{-3}.

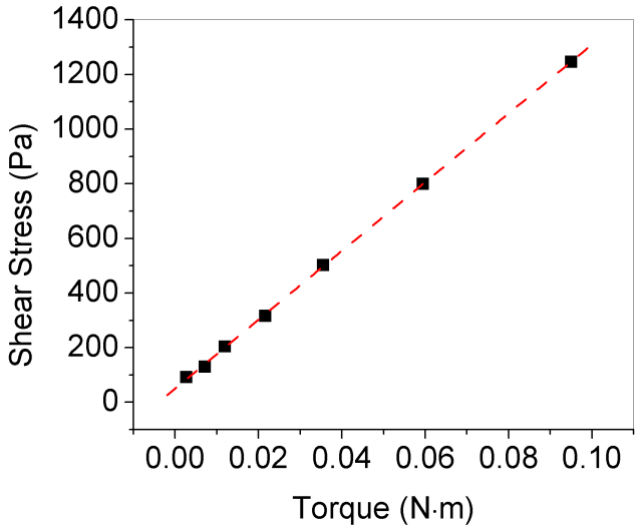

Figure 3.26 Calibration curve using the calibration fluid with a viscosity of 5,237 mPa·s

3.4.3 Validation of Rheometer

The developed rheometer is evaluated using a calibration fluid and PDMS at room temperature in steady shear and sinusoidal oscillation modes. The results with and without the dynamic seal are presented to determine whether the friction correction schemes that were previously discussed are valid.

In the steady shear mode, each viscosity is calculated by dividing the measured shear stress by the shear rate. The shear stress is measured twice for each shear rate and averaged. The viscosity of the calibration fluid over a range of shear rates is shown in Figure 3.27. The results

show that the viscosity when the dynamic seal is used resulted in a much closer value to the actual viscosity of the calibration fluid (5,237 mPa·s) than when the dynamic seal was not used. The viscosity was also relatively constant over the investigated shear rate range, which was expected for the Newtonian fluid. Without the seal, the viscosity was slightly overestimated at lower shear rates (~6,000 mPa·s), and it approached a value close to the actual viscosity at higher shear rates. The steady shear results for PDMS are shown in Figure 3.28 . Since PDMS is a typical shear-thinning fluid, it is expected that the viscosity is constant at lower shear rates (Newtonian plateau region) and that it decreases at higher shear rates (power-law region). Although the viscosity of the PDMS is unknown, viscosity in the Newtonian plateau region can be approximated by dividing the kinematic viscosity (12,500 cSt) by the density (0.975 at 25°C), which results in 12,821 mPa·s. Similar to the case of the calibration fluid, with the seal, the viscosity was much closer to the value of the actual viscosity compared to the case when no seal was used; therefore, without the seal, in this case the viscosity was underestimated. PDMS did not show distinctive shear-thinning behavior within the range of the investigated shear rates. From the above observations, the steady shear measurement with the seal gives a reasonably accurate viscosity value. This result demonstrates that the torque correction scheme discussed in the previous section is valid.

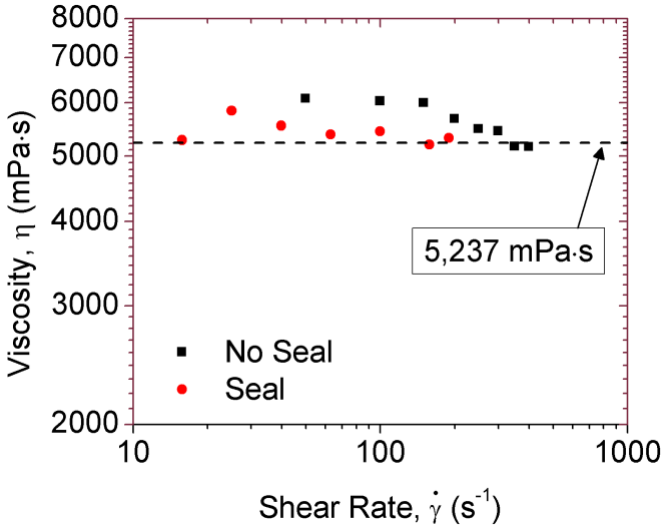

Figure 3.27 Viscosity of the calibration fluid measured with and without the dynamic seal

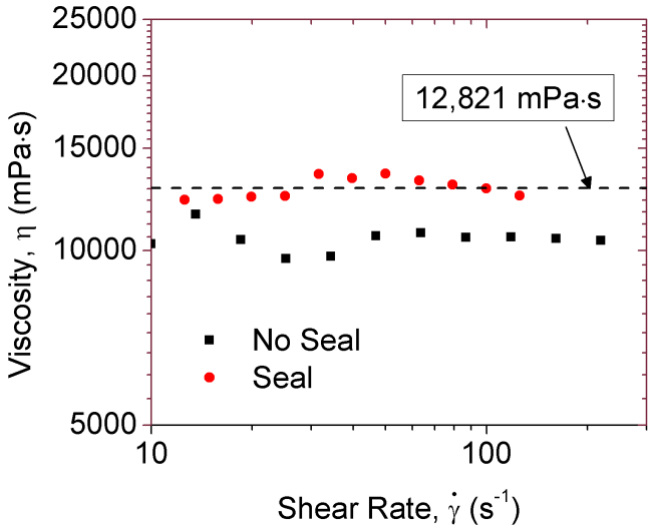

Figure 3.28 Viscosity of the PDMS measured with and without the dynamic seal

In sinusoidal oscillation, there are two modes of operation: strain sweep and frequency sweep. Strain sweep tests are usually conducted prior to the frequency sweep to determine the critical strain for linear viscoelasticity for a test fluid. The strain should not exceed the critical strain to ensure the measurements are within a linear viscoelastic range. The strain sweep test was performed without the dynamic seal to minimize the measurement error. The strain sweep

test results using the calibration fluid at 6.28 and 62.8 rad/s at various strain amplitudes are shown in Figure 3.29. The calibration fluid did not show any significant decrease in the magnitude of the complex modulus (|G*|) within the investigated amplitude range (up to 50 strain for 6.28 rad/s and 5 strain for 62.8 rad/s). This result meant that the strain amplitude of 5 was well below the critical strain at a frequency of 62.8 rad/s or below. Therefore, a strain amplitude of 5 was used in the frequency sweep tests for frequencies up to 62.8 rad/s.

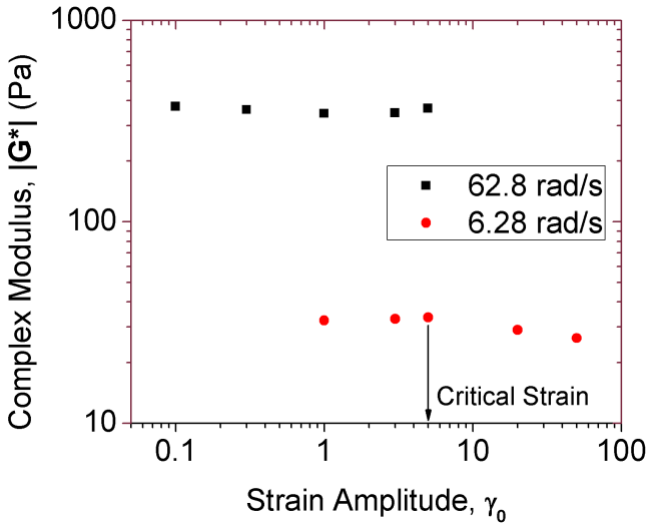

Figure 3.29 Strain sweep test using the calibration fluid

For the PDMS, strain sweep tests were performed at 6.28, 19.9, 62.8, 199, and 314 rad/s (Figure 3.30). PDMS did not show any significant decrease in the |G*| at 62.8, 199, and 314 rad/s. In contrast, the |G*| decreased at strains above 6.3 for 19.9 rad/s and above 10 for 6.28 rad/s. From the point where the complex viscosity starts to decrease, the internal structure of PDMS fractured, and PDMS did not behaves like a Newtonian fluid. Based on the strain sweep results, the strain amplitudes used for the frequency sweep tests are shown in Table 3..

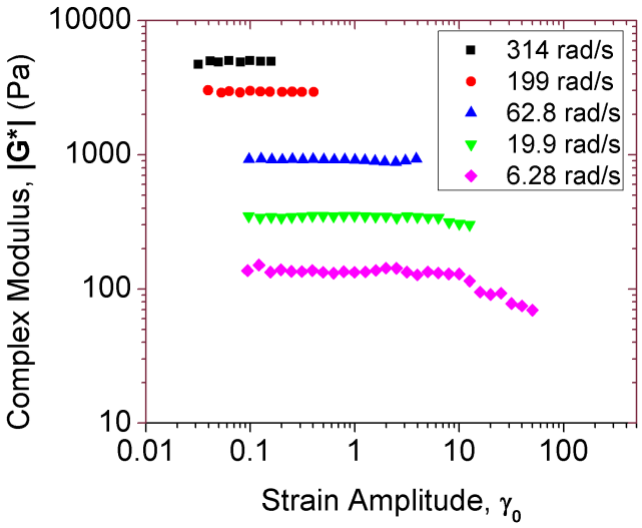

Figure 3.30 Strain sweep test using PDMS

Table 3.4 Strain amplitudes used for frequency sweep tests for the calibration fluid and PDMS

Sample	**Angular frequency range (rad/s)**				
	6.28 or less	**6.28 – 19.9**	**19.9 – 62.8**	**62.8 – 199**	**199 – 314**
PDMS	10.0	6.3	3.8	0.4	0.16
Calibration fluid	5.0			-	-

Frequency sweep is performed with and without the dynamic seal using the strain amplitudes determined from the amplitude sweep experiments. Figure 3.31 shows the dependency of the loss modulus *G''* and the storage modulus *G'* on frequency. *G''* is larger than *G'*, which means that viscous behavior is more dominant than elastic behavior within the investigated shear rate range. The frequency dependency is more pronounced in *G'* than in *G''* and a crossover point is predicted at higher frequencies. This trend is the same as the observations of other studies (Kissi et al. 1992; Ghannam and Esmail 1998). Although *G'* and *G''* show a similar overall trend in both cases (with and without the seal), with the seal, *G'* is

significantly larger than *G'* measured without the seal. This discrepancy is mainly due to the deviation in the value of the phase difference. The phase differences measured at various frequencies are listed in Table 3.5. Without the seal, the phase difference was close to 90° up to a frequency of 6.28 rad/s, and it gradually decreased at higher frequencies. This result was consistent with the trend observed in typical polymeric liquids. The results using the seal exhibited a similar trend, but the overall values were smaller than those in the case when the seal was not used. Since *G'* was the product of the complex modulus and cos δ, a small difference in δ near 90° resulted in a significant change in G'. For example, cos85° was five times larger than cos 89°.

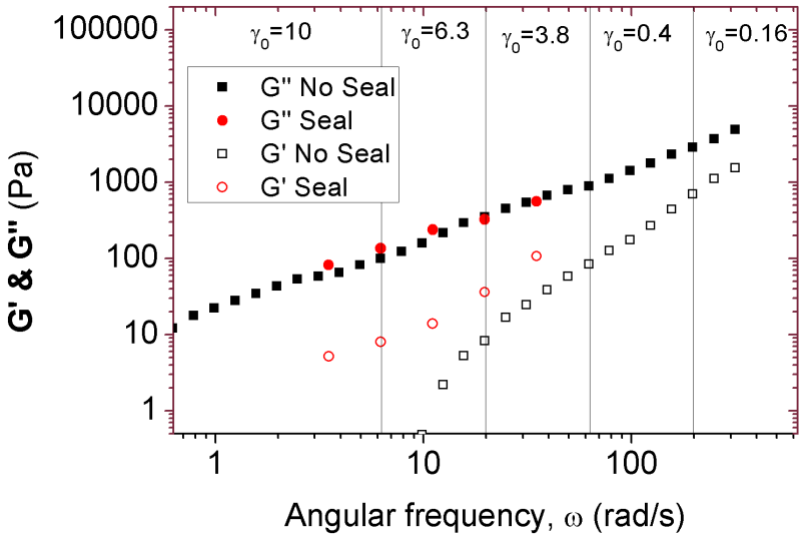

Figure 3.31 Storage and loss modulus (*G'* and *G''*) of the PDMS measured with and without the dynamic seal

Table 3.5 Change in the phase difference depending on the frequency

Angular Frequency, ω (rad/s)	**Phase difference, δ (°)**	
	PDMS	
	No Seal	**Seal**
0.628	96.2	-
0.791	90.3	-
0.996	91.0	-
1.25	89.5	-
1.58	91.3	-
1.99	90.8	-
2.50	90.7	-
3.15	90.8	-
3.53	-	86.4
3.96	90.1	-
4.99	90.1	-
6.28	89.9	86.6
7.91	90.0	-
9.96	89.8	-
11.2	-	86.7
12.5	89.4	-
15.8	89.0	-
19.9	88.6	83.7
25.0	87.9	-
31.5	87.4	-
35.3	-	79.2
39.6	86.7	-
49.9	85.8	-
62.8	84.6	-
79.1	83.6	-
99.6	83.0	-
125	81.4	-
158	79.2	-
199	76.3	-
250	73.1	-
315	72.6	-

There are several possible reasons for this deviation. First, the strain profile is not a complete sinusoidal profile due to the excessive friction of the seal. There is always some distortion, especially at the peak strain (where the rotational direction changes). Second, the frictional torque measured without any liquid cannot exactly match the frictional torque when a fluid is present. Nevertheless, the results when the seal was used can provide reliable information in terms of the relative change in the viscoelasticity of a fluid.

The magnitude of the complex viscosity $|\eta^*|$ is shown in Figure 3.32. The $|\eta^*|$ is distributed between 14,000 and 22,000 mPa·s without showing any consistent trend. In fact, it is widely accepted that the complex viscosity has a close relationship with the shear viscosity η:

$$|\eta^*(\omega)| = \eta(\dot{\gamma}) \text{ with } \omega = \dot{\gamma} \qquad (3.11)$$

where ω is angular frequency. This empirical relationship is called the "Cox-Merz rule" (Cox and Merz 1958) and has been found to be true for most of the polymer melts. Therefore, the deviation of $|\eta^*|$ from the value of the steady shear viscosity η (12,821 mPa·s) can be regarded as a measurement error.

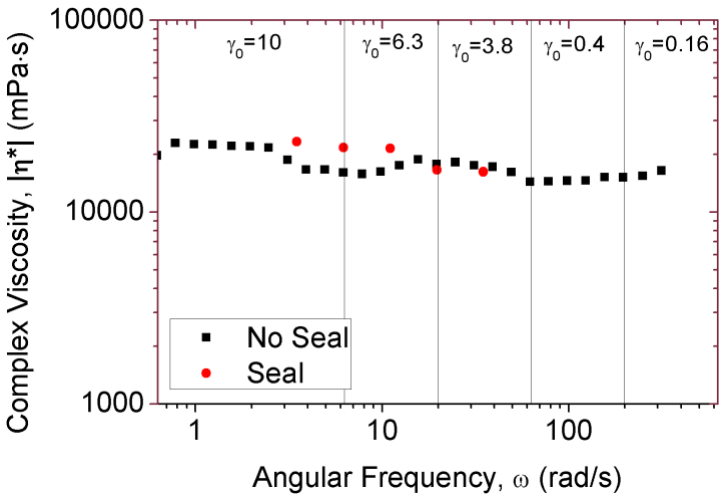

Figure 3.32 Magnitude of the complex viscosity ($|\eta^*|$) of the PDMS measured with and without the dynamic seal

3.5 Summary

The overall design and some major components of the developed rheometer were presented in this chapter. One of the main characteristics of the developed rheometer was the use of the piezoelectric torque dynamometer. The piezoelectric torque dynamometer had exceptional linearity over a wide range of torque values, superiority in dynamic measurements, and was less dependent on temperature. The developed rheometer also utilized the dynamic shaft seal, which allowed for rheological measurements under high pressure. The torque dynamometer was calibrated to determine the transducer sensitivity and scale factor for a charge amplifier. The temperature control, motion control, data acquisition, and bearing/shaft seal were also described in detail. The effect of the distance between the cylinder bottoms on the torque measurement was investigated to find the minimum distance where the end effect was negligible. The rheometer was then calibrated using the calibration fluid with known viscosity to find the correlation between torque and shear stress. The friction correction schemes for each modes of operation were also presented.

The operation of the developed rheometer was validated using the calibration fluid and PDMS in each mode of operation at room temperature. The rheological measurements were conducted with and without the dynamic seal to validate the effectiveness of the friction correction schemes. In the steady shear mode, using the dynamic seal and the correction scheme resulted in accurate viscosity measurements. In the sinusoidal oscillation mode, it was demonstrated that G', G'', and $|\eta^*|$ could be measured between 0.628 and 315 rad/s (without the seal) and 3.52 and 35.2 rad/s (with the seal).

CHAPTER 4: EXPERIMENTAL RESULTS AND MODELING

In this chapter, the effects of temperature and dissolved CO_2 on the rheological properties of PDMS are investigated using the developed rheometer in both steady shear and sinusoidal oscillation mode. The effects of the individual parameters on the viscosity are experimentally investigated and correlated using several models. The prediction of the amount of dissolved CO_2 at a given temperature and pressure is also presented. Then, empirical models are proposed that account for the combined effect of temperature and pressure on the viscosity. One of the main advantage of the proposed models is that the viscosity can be predicted at a given temperature and pressure without knowing the volumetric properties of the pure components and the mixture. In addition to the viscosity measurement, the dynamic rheological parameters are also measured at various temperatures and CO_2 saturation pressures. The capability and the limitations of the developed system are also discussed.

4.1 Steady Shear Measurement

4.1.1 Effects of Temperature

Steady shear measurements were conducted using PDMS at various shear rates and temperatures at 25°C, 50°C, and 80°C. Sufficient time was allowed before measuring for the system to be in the thermal equilibrium state. The results are shown in Figure 3.17. It was observed that the viscosity of the PDMS was highly sensitive to temperature variations. It was also observed that the PDMS exhibited the behavior of a Newtonian fluid within the temperature and shear rate range investigated. The viscosity data at a lower shear rate range was ignored because there was a noticeable deviation from the Newtonian behavior. At lower shear rates, the

torque generated by the fluid became too small compared to the torque generated by the friction of the seal causing a large experimental error. The threshold shear rate was further reduced at higher temperatures due to the low viscosity of the fluid.

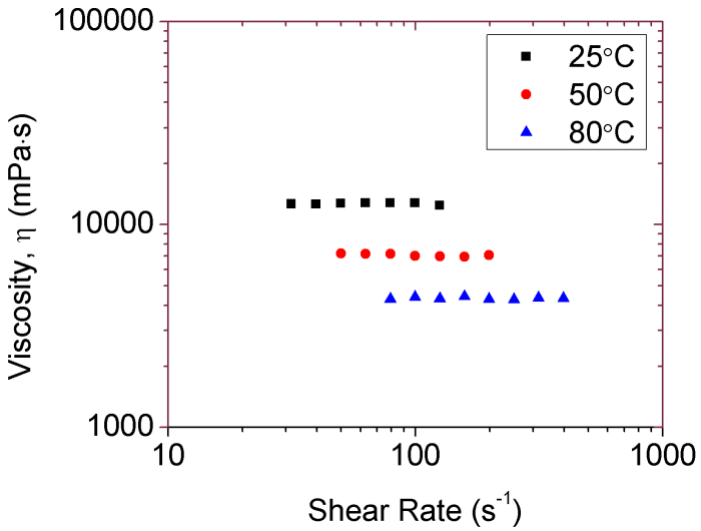

Figure 4.17 Steady shear viscosity of pure PDMS as a function of shear rate at three temperatures

The variation in viscosity due to temperature change was quantitatively described using two models: the William-Landel-Ferry (WLF) equation (Williams et al. 1955) and Arrhenius type equation (Barus 1893), often expressed as the following equations:

$$\text{WLF: } \log\left(\frac{\eta}{\eta_0}\right) = \frac{C_1(T - T_0)}{C_2 + T - T_0} \tag{4.12}$$

$$\text{Arrhenius: } \eta = \eta_0 \exp\left[\frac{E_0}{R}\left(\frac{1}{T} - \frac{1}{T_0}\right)\right] \tag{4.13}$$

where η is the viscosity at temperature T, η_0 is the viscosity at a reference temperature T_0, and R is the gas constant. The viscosity at each temperature was averaged to get η, and the average viscosity at 25°C (T_0) was used for η_0. C_1 and C_2 are the WLF parameters, and E_0 is the

activation energy for flow, which needs to be determined experimentally. WLF parameters can be obtained by rearranging equation (4.12) as follows:

$$-\frac{1}{\log(\eta/\eta_0)} = \frac{C_2}{C_1}\frac{1}{T-T_0} + \frac{1}{C_1} \qquad (4.14)$$

Plotting -1/log(η/η_0) versus 1/(T-T_0), C_1 and C_2 can be determined by finding the best linear fit of the experimental data as shown in Figure 3.18. The activation energy E_0 for the Arrhenius type equation can also be similarly determined as shown in Figure 3.19. The experimentally determined parameters are listed in Table 3.5.

Table 4.7 Parameters of the WLF and Arrhenius equations.

WLF		**Arrhenius**	**Reference**
C_1	**C_2**	***E_0* (kJ/mol)**	
1.54	126	17.5	This study
1.90	222	-	Barlow et al. (1964)

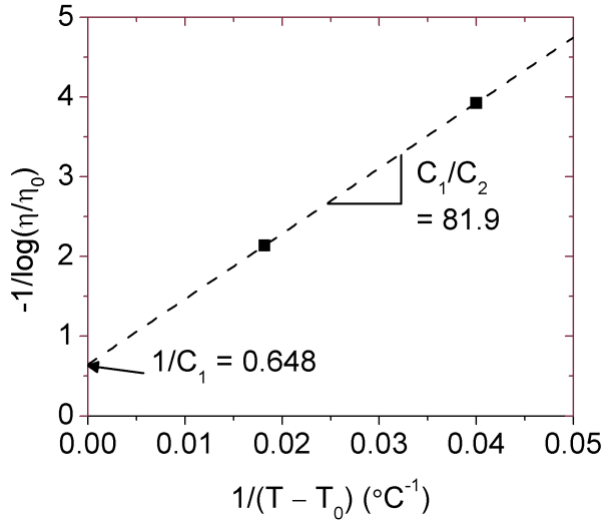

Figure 4.18 Plot of -1/log(η/η_0) vs. 1/(T-T_0) to calculate the C_1 and C_2 from the experimental data

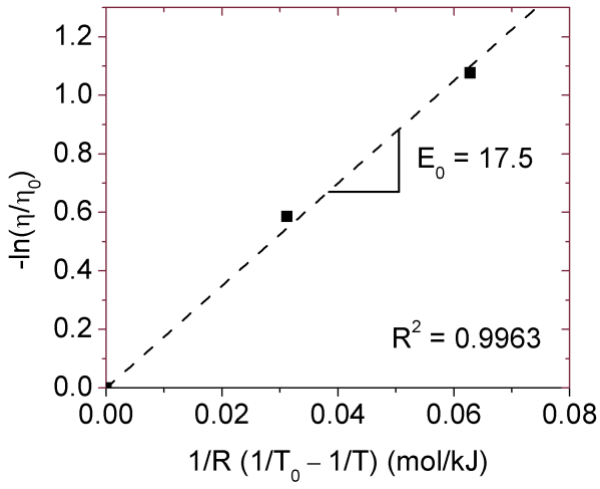

Figure 4.19 Plot of -ln(η/η_0) vs. 1/R (T_0-T) to calculate the E_0 from the experimental data

The experimentally measured viscosity along with the fitted lines for the two models are depicted in Figure 3.20. Viscosity of PDMS was reduced by 44.4% at 50°C and 65.9% at 80°C compared to the viscosity at the reference temperature. Both models showed excellent agreement with the experimental data while the WLF correlation provided a slightly better fit to the experimental data.

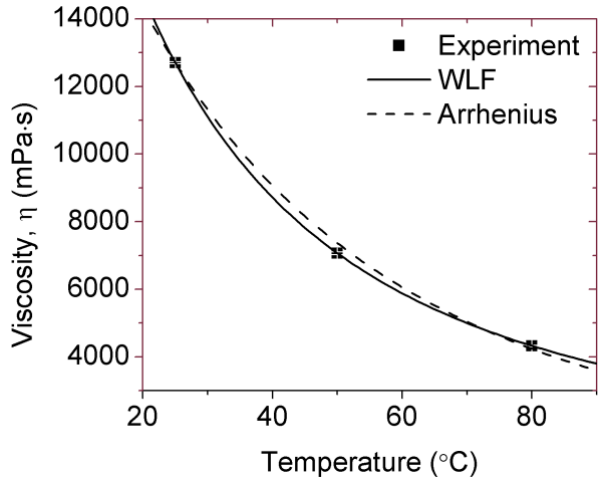

Figure 4.20 Viscosity of pure PDMS at various temperature with best-fit WLF and Arrhenius correlations. The reference temperature, T_0, is 25°C.

4.1.2 Effects of Dissolved CO_2

High pressure measurements were performed in the steady shear mode to evaluate the effect of dissolved CO_2 on the viscosity of the PDMS. The rheometer was first purged with CO_2 for 10 minutes to replace air in the pressure cell to CO_2 and then pressurized using a high pressure regulator to a desired pressure. The viscosity was periodically monitored during the dissolution process until no further viscosity reduction is observed to ensure the complete saturation of the CO_2 in the PDMS.

Viscosities of the PDMS-CO_2 at various shear rates at temperature of 50°C and pressure up to 3 MPa are shown in Figure 4.21. It was observed that the viscosity of the PDMS is highly sensitive to the pressure variation similar to that was observed for temperature variation. It was also observed that the PDMS exhibits behavior of Newtonian fluid within the pressure and shear rate range investigated. It should be noted that the maximum shear rate is significantly reduced at the higher pressures. This is due to the increased friction at the dynamic seal at higher pressures, thus causing the motor torque limit is reached at much lower shear rates. The dashed line indicates the minimum viscosity that can be measured accurately at given shear rates which corresponds to the torque of 20 mN·m. Viscosity data below this line showed large experimental scatter. The measurement fluctuation within the measurement range was about ±5%.

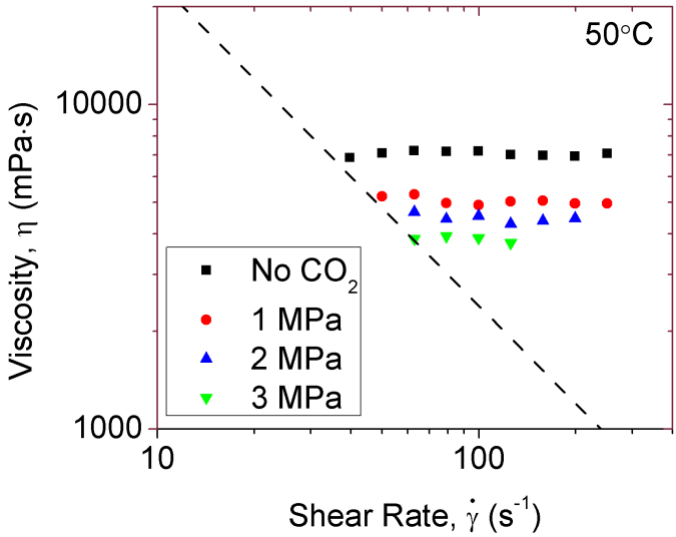

Figure 4.21 Steady shear viscosity of PDMS-CO_2 as a function of shear rate at various saturation pressures

Estimation of the amount of dissolved CO_2 in PDMS

In this study, the amount of dissolved CO_2 in the PDMS was not measured, but instead estimated using solubility data from other literature and making several assumptions. The assumptions are; 1) PDMS is fully saturated with CO_2, and 2) the amount of the dissolved CO_2 is proportional to the pressure (Henry's law). The dissolved concentration of CO_2, w_c, can be expressed using Henry's law which is given by the following equation:

$$w_c = HP \tag{4.15}$$

where H is the Henry's solubility constant and P is the equilibrium pressure. The solubility of CO_2 in PDMS was measured by Xu et al. at various temperatures and pressure ranging up to 10.1 MPa (Xu et al. 2009). In Figure 4.22, the solubility data at various temperatures are plotted up to the pressures of 2.0 or 3.0 MPa where the solubility increases linearly with pressure. Henry's solubility constants for each temperature were determined from the slop of the dotted lines in the

plot and they are listed in Table 3.6. The temperature dependency of the Henry's solubility constant is generally expressed in the following form (Smith and Harvey 2007):

$$H(T) = H_0 \exp\left[-\frac{E_s}{R}\left(\frac{1}{T} - \frac{1}{T_0}\right)\right] \tag{4.16}$$

where T_0 is the reference temperature (35°C in this case), H_0 is the Henry's constant at T_0, and E_s is the enthalpy of dissolution. E_s can be determined by plotting $\ln(H/H_0)$ versus $1/R\ (1/T - 1/T_0)$ as shown in Figure 4.23 (E_s = -11.8).

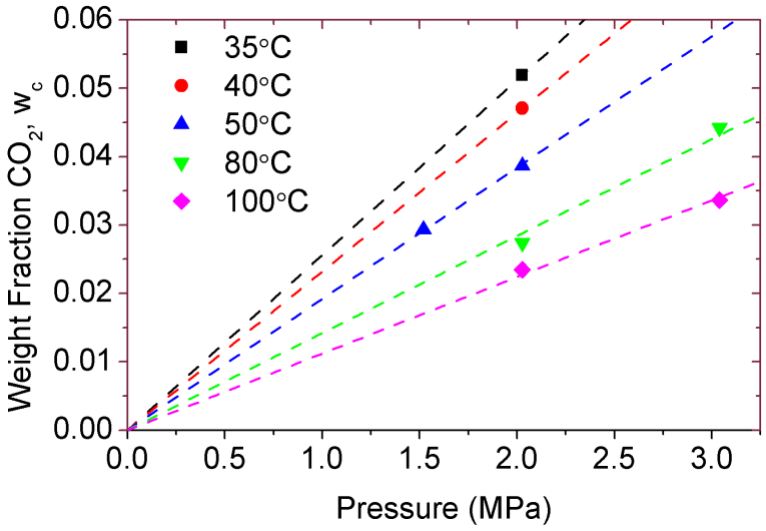

Figure 4.22 Equilibrium solubility of CO_2 in PDMS at various temperatures (Xu et al. 2009)

Table 4.8 Henry's solubility constant at various temperatures

Temperature (°C)	**35**	**40**	**50**	**80**	**100**
***H* (MPa^{-1})**	2.56E-2	2.32E-2	1.92E-2	1.42E-2	1.12E-2

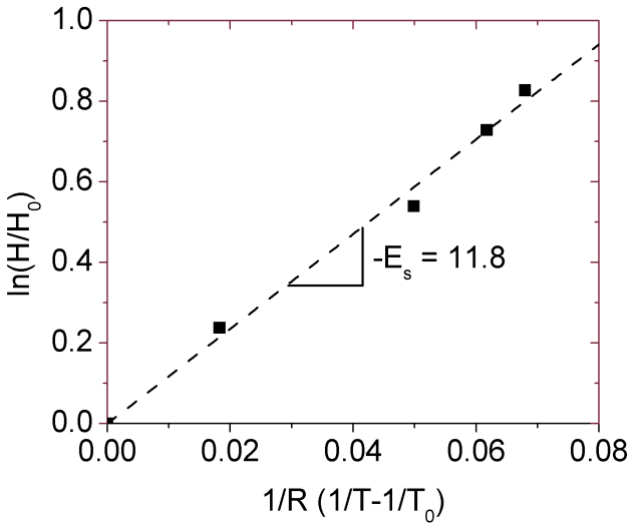

Figure 4.23 Plot of $\ln(H/H_0)$ vs. $1/R\ (1/T-1/T_0)$ to calculate the E_s from the experimental data

By substituting the equation (4.16) into equation (4.15) and using the determined parameters, weight fraction of CO_2 in the PDMS at a given temperature and pressure can be predicted using the following equation:

$$w_c(T,P) = 0.0256\exp\left[1.41\times10^3\left(\frac{1}{T}-\frac{1}{308.15}\right)\right]P \qquad (4.17)$$

Effect of dissolved CO_2 on the viscosity of PDMS

Using the above equation, the weight fractions of CO_2 under the experimental conditions were calculated. The average viscosity as a function of weight fraction of CO_2 is shown in Figure 3.21 along with several models. One of the models is a simple exponential equation proposed by Yeo and Kiran (1999) which is given by:

$$\eta = \eta_{0,w_c}\exp(Bw_c) \qquad (4.18)$$

where η_{0,w_c} is the viscosity of the pure polymer and *B* is a constant. This model showed noticeable deviation from the experimental results. The poor agreement led us to add a second order term in the exponent:

$$\eta = \eta_{0,w_c} \exp(Bw_c + Cw_c^{\,2}) \tag{4.19}$$

where the *C* is also a constant. Although this model provided a better fit to the experimental data, there is no physical significance in *B* and *C*. Another model considered in this study is the equation proposed by Fujita and Kishimoto (1958) which is given by:

$$\ln\left(\frac{\eta}{\eta_{0,w_c}}\right) = \frac{(-1/f)w_c}{f/\theta + w_c} \tag{4.20}$$

where *f* is the fractional free volume and θ is the parameter representing the contribution of the dissolved gas in increasing the free volume. In this study, the *f* and θ are considered as adjustable parameters. Rearranging equation (4.20) yields:

$$\frac{1}{\ln(\eta/\eta_{0,w_c})} = \frac{f^2}{\theta}\frac{1}{w_c} + f \tag{4.10}$$

f and θ can be obtained by plotting $1/\ln(\eta/\eta_{0,w_c})$ versus $1/w_c$ as shown in Figure 3.26. The Fujita-Kishimoto equation showed good agreement with the experimental data. The model parameters determined for each predictive model are presented in Table 3..

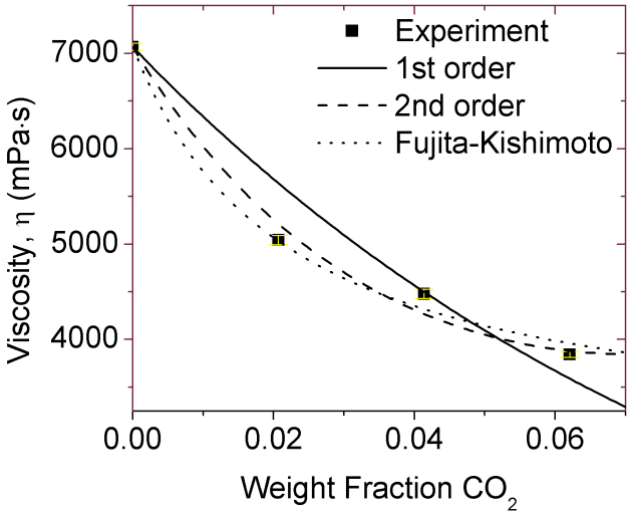

Figure 4.24 Viscosity of PDMS at various weight fraction of CO_2 and 50°C along with several predictive models.

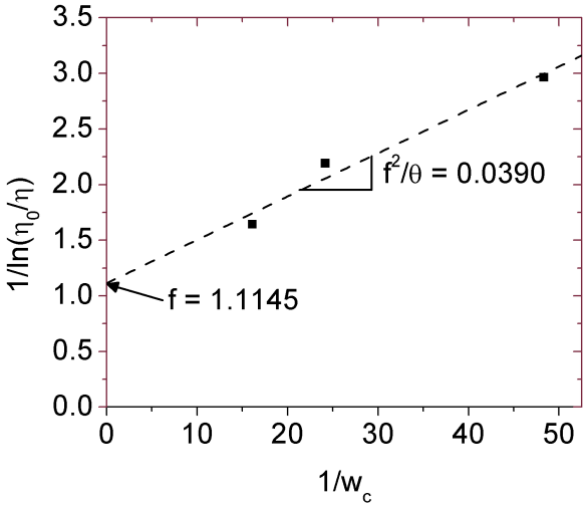

Figure 4.25 Plot of $1/\ln(\eta/\eta_{0,w_c})$ vs $1/w_c$ as to calculate the f and θ from the experimental data

Table 4.9 Parameters of the models that account for the CO_2 concentration

Yeo and Kiran	**Exponential w/ 2nd order polynomial**		**Fujita-Kishimoto**	
B	**B**	**C**	f	θ
-10.9	-17.2	122	1.11	32.8

Figure 3.22 shows the relative change of the viscosity of the PDMS as a function of weight fraction of CO_2 at 50°C. The data of Gerhardt et al. (1997) obtained using a capillary extrusion rheometer is also presented for comparison. Both data show reasonable agreement thus confirming the validity the developed rheometer. Small deviations between the two study can be attributed to the different molecular weight of the PDMS. Gerhardt et al. used higher molecular weight PDMS (M_w=308,000 g/mol) in comparison with this study (Mw=95,000 g/mol).

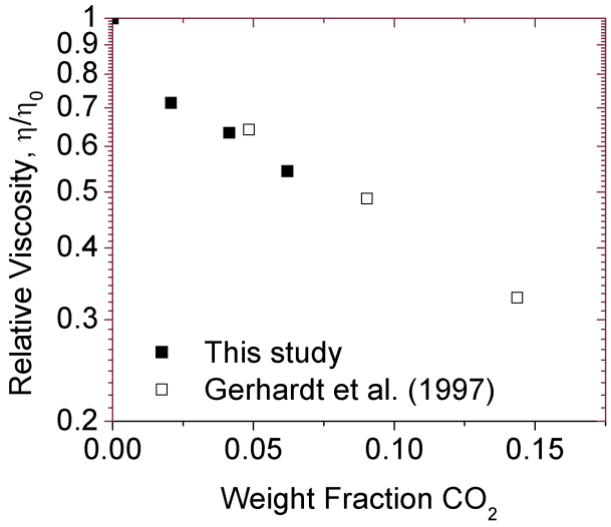

Figure 4.26 Effect of the weight fraction of CO_2 on relative viscosity of PDMS

4.2 Modeling

The combined effects of temperature and pressure on the viscosity of the PDMS-CO_2 system were investigated. Although there have been numerous attempts to predict viscosity of polymer-gas system, most of the proposed models require volumetric parameters (e.g. specific volume and occupied volume) of the individual components and the mixture which are difficult to measure. Prediction of these volumetric parameters is also challenging because of the complex thermodynamic concept involved and requires physical and thermodynamic properties of the materials. Therefore, these approaches are lack of practical significance and cannot be readily

used for predicting viscosity at certain processing conditions. In order to avoid the difficulties, a viscosity prediction model based on empirical approach was developed. It will be shown that the viscosity of the PDMS-CO_2 can be expressed as a function of temperature and pressure.

Viscosity of polymer-gas system has been expressed mathematically in terms of temperature (T), pressure (P), and weight fraction of dissolved gas (w_c) using the following form which is known as generalized Arrhenius equation (Lee et al. 1999; Ladin et al. 2001):

$$\eta(T,P,w_c) = A\exp\left[\frac{\alpha}{T-T_r} + \beta P + \psi w_c + (higher\ order\ terms)\right] \qquad (4.21)$$

where A, α, T_r, β, and ψ are constants. By dropping the higher order terms and the pressure term (assuming that the pressure has negligible effect on the viscosity), equation (4.21) becomes:

$$\eta(T,w_c) = A\exp\left[\frac{\alpha}{T-T_r} + \psi w_c\right] \qquad (4.22)$$

Equation (4.22) can be further modified by replacing the temperature related term with the Arrhenius type equation (4.13) because they both are in exponential form:

$$\eta(T,w_c) = A\exp\left[\frac{E_0}{R}\left(\frac{1}{T}-\frac{1}{T_0}\right) + \psi w_c\right] \qquad (4.23)$$

The empirical constants A, α, T_r, E_0, and ψ were determined using a least-square method based on the Trust-Region algorithm. Using this algorithm, the constants were successfully determined as shown in Table 4.10.

Table 4.10 Parameters of the models of the temperature and the gas concentration dependency

Generalized Arrhenius model				**Modified generalized Arrhenius model**		
A	***T_r***	***α***	***ψ***	***A***	***E_0***	***ψ***
593	-76.5	311	-11.6	1.26E4	18.3	-12.2

By substitute equation (4.17) into the both models, viscosity can be expressed as a function of temperature and pressure. The experimentally measured viscosity and the predicted viscosity using the two models are shown in Figure 3.23 and Figure 3.24. Both models showed good agreement with the experimental data and they could describe the effect of the temperature and CO_2 saturation pressure on the viscosity of PDMS-CO_2.

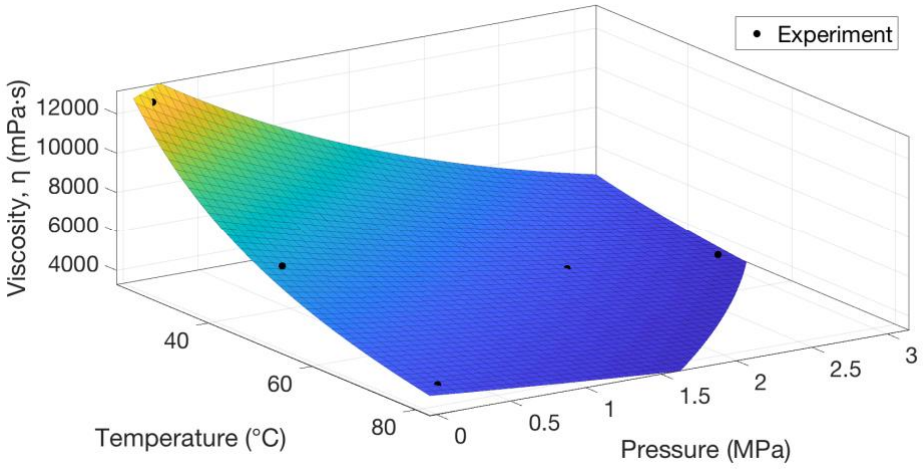

Figure 4.27 Viscosity as a function of temperature and pressure predicted using the generalized Arrhenius equation

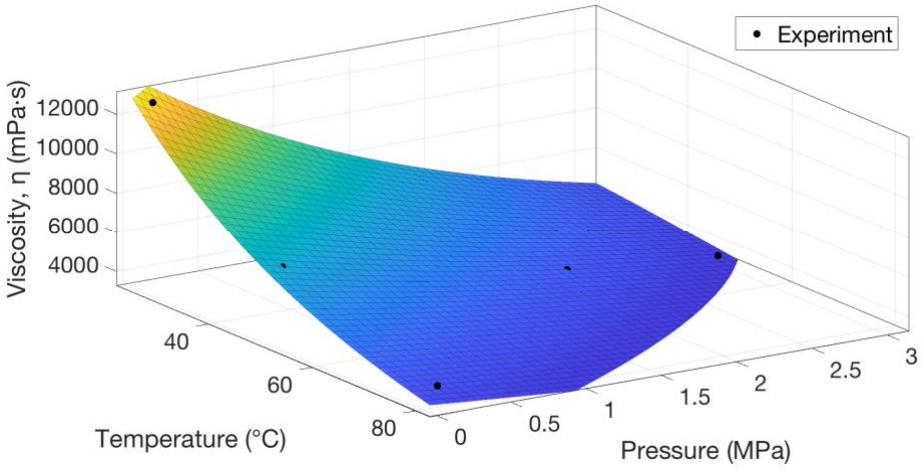

Figure 4.28 Viscosity as a function of temperature and pressure predicted using the modified generalized Arrhenius equation

4.3 Sinusoidal Oscillation Measurement

Sinusoidal oscillation tests were performed at various frequencies using the pure PDMS and PDMS-CO_2 to measure dynamic modulus (G' and G'') and complex viscosity ($|\eta^*|$). The strain amplitudes, that have been determined in the previous chapter, were used in order to ensure that the measurements are conducted within the linear viscoelastic range.

The dynamic modulus and complex viscosities of the PDMS at various temperatures without CO_2 are shown in Figure 3.25 and Figure 3.27. It is clearly shown that the loss modulus and complex viscosity decrease as the temperature increases. However, the developed rheometer failed in providing reliable measurement of the storage modulus due to the high uncertainty in evaluating the phase difference (δ). Moreover, the complex viscosity varied significantly with the frequency which is different from the expectation. These experimental errors can be attributed to the uncertainty of the friction at the dynamic seal.

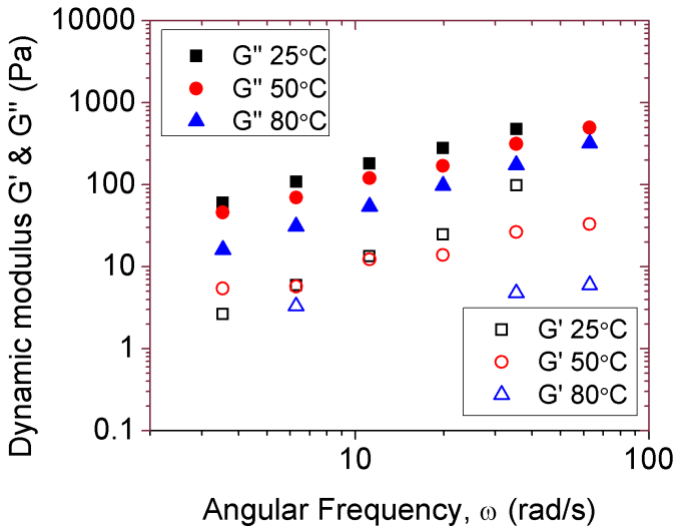

Figure 4.29 Dynamic modulus of pure PDMS as a function of frequency at various temperatures

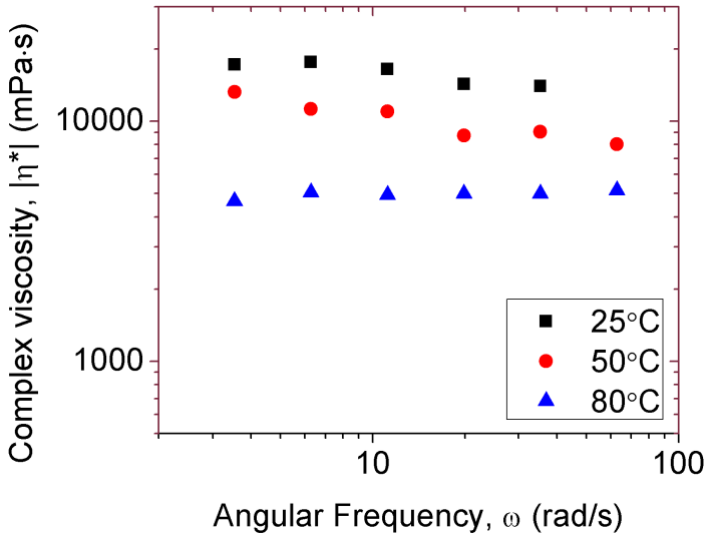

Figure 4.30 Complex viscosity of pure PDMS as a function of frequency at various temperatures

The dynamic modulus and complex viscosities of the PDMS at various CO_2 saturation pressure are also shown in Figure 3.28 and Figure 3.29. Decrease in the loss modulus and complex viscosity was observed as the CO_2 saturation pressure increases. However, the high degree of uncertainty was also observed in the storage modulus.

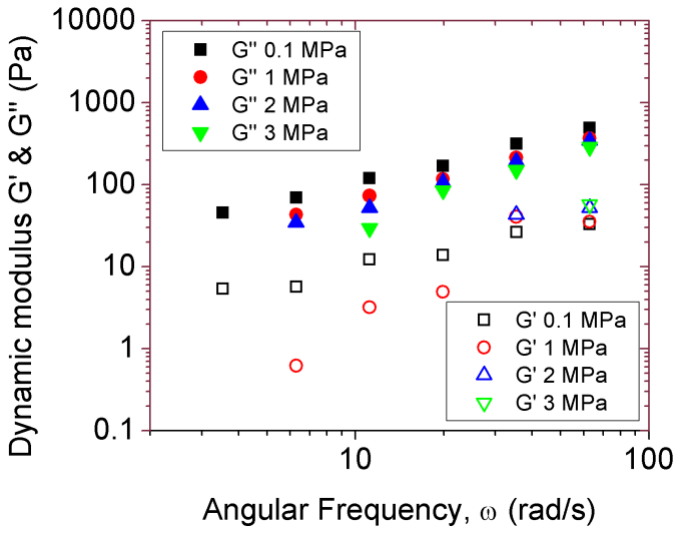

Figure 4.31 Dynamic modulus of pure PDMS as a function of frequency at various CO_2 saturation pressures

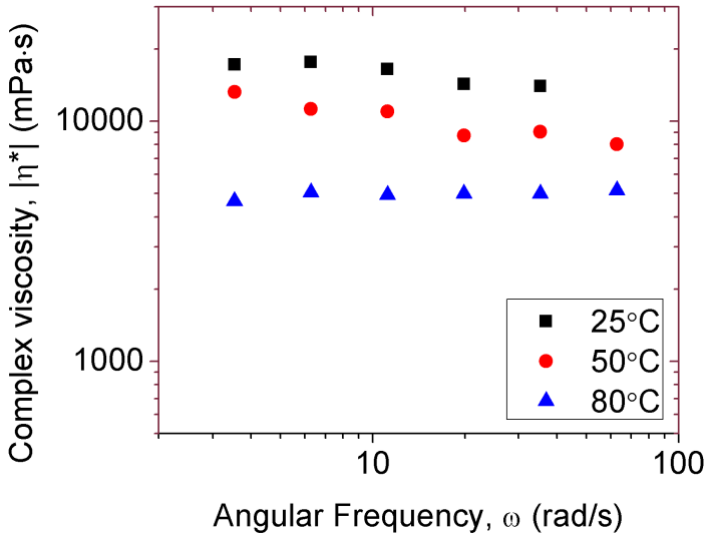

Figure 4.32 Complex viscosity of pure PDMS as a function of frequency at various CO_2 saturation pressures

Overall, the developed rheometer could give information on how the dynamic rheological parameters are changed at various temperature and CO_2 saturation pressure in general. It was shown that the increase of temperature and saturation pressure resulted in decreased loss modulus and complex viscosity. However, the change of the storage modulus could be not clearly distinguished due to the experimental error.

4.4 Summary

This chapter presented the effects of temperature, pressure, and dissolved CO_2 on the rheological parameters of the PDMS. Viscosities of PDMS at various temperature and CO_2 saturation pressure were successfully measured using the developed rheometer. The temperature dependency was found to fit both WLF and Arrhenius equation. The amount of dissolved CO_2 at the corresponding pressure and temperature was estimated using Henry's law. The Fujita-Kishimoto equation and the exponential equation whose exponent contains the second order

polynomial were the most suitable equation in describing the effect of the dissolved CO_2 on the viscosity. The combined effect of the temperature and the CO_2 saturation pressure was modeled using empirical models based on the generalized Arrhenius type equation. Using this model viscosity of PDMS-CO_2 could be expressed as a function of temperature and pressure. The dynamic rheological parameters, determined from the sinusoidal oscillation measurements, showed the similar trend as the viscosity measurement. Although the general trend of the *G''* and the complex viscosity (higher temperature and CO_2 saturation pressure reduced the *G''* and the complex viscosity) could be observed, it was not possible to obtain reliable measurement of the *G'* due to the high uncertainty of friction of the seal.

CHAPTER 5: CONCLUSION

Understanding the rheological properties of materials under high pressure is important because various industrial processes operate under high pressure. However, many studies on the high pressure rheology have been relied on pressure-driven rheometers or falling ball rheometers that have limited capability in term of performing various rheological measurement. Several studies have developed high pressure rotational rheometers, but they have limited capability in dynamic rheological measurement due to the inertia and compliance of the torque transducer they used. In this thesis, a concentric cylinder rheometer was developed that was designed to perform high pressure rheological measurements. Effects of temperature and pressure on the rheological properties of PDMS-CO_2 system were investigated using the developed rheometer. In this chapter, a summary and the novel contributions of the presented work are provided. Furthermore, the assumptions and limitations of the experiments and modeling are discussed followed by suggestions for possible future work.

5.1 Summary

In this thesis, a high pressure rotational was designed, fabricated, and calibrated for taking rheological measurements of viscoelastic fluids. The concentric cylinder was adopted to minimize errors associated with the fluid volume swelling, which was caused by dissolving gas in the fluids under high pressure. The closed chamber design of the concentric cylinder and using a dynamic seal for the shaft of the inner cylinder enabled the pressurization of gas up to 3 MPa. The inner cylinder was driven by a brushless DC motor to impose a steady and sinusoidal oscillating strain. The outer cylinder was mounted on a piezoelectric torque dynamometer, which

measured the torque at high sampling rates up to 1000 Hz. Calibrating the torque dynamometer was done using a hammer instrumented with a force sensor. The effect of the cylinder bottom (i.e., the end-effect) was evaluated at various distances, and the optimum distance was determined to be 3.2 mm. The effect of seal friction on the torque measurement was also evaluated by rotating an empty cylinder at each mode of operation. Friction was found to vary depending on the operating conditions, and it could be successfully evaluated and compensated for by subtracting the friction values from the total torque signal. The entire system was calibrated using a calibration fluid with a viscosity of 5,237 mPa·s, and the calibration coefficient was determined to be 12,583 m^{-3}, which had excellent proportionality.

The operation of the developed rheometer was validated using PDMS with and without the seal. In the steady shear mode, the viscosity was measured at various shear rates. PDMS showed Newtonian behavior within the range of shear rates investigated. The measured viscosity with the seal agreed well with the actual viscosity of the PDMS; this result demonstrated the validity of the proposed friction compensation scheme. In the sinusoidal oscillation mode, strain sweep tests were performed without the seal to minimize the signal distortion caused by friction. The critical strains for each frequency level were clearly identified. Using the critical strain values, a frequency sweep test was performed to obtain the dynamic rheological parameters with and without the seal. The dynamic modulus (i.e., storage modulus *G'* and loss modulus *G''*) followed the general trend of typical polymeric liquids in both cases.

The effect of temperature and CO_2 saturation pressure on the rheological parameters of PDMS was then investigated using the developed rheometer. First, the viscosity was measured at various temperatures and shear rates at atmospheric pressure without CO_2. The viscosity of PDMS did not show any shear rate dependency within the shear rate range investigated, and the

temperature dependency was well described by WLF and Arrhenius equation. Then, the viscosity of a PDMS-CO_2 system was measured at a fixed temperature, and a 47.3% reduction in viscosity was observed at 3 MPa. The solubility of CO_2 in PDMS was expressed as a function of temperature and pressure using the solubility data found in the literature. The viscosity was expressed as a function of temperature and pressure by combining the solubility equation with the empirical models based on generalized Arrhenius equation.

5.2 Contributions

This research introduces the design of a high pressure rotational rheometer that utilizes a piezoelectric torque transducer and other methods to evaluate rheological parameters. The novel scientific contributions are listed in this section.

i. *Using a piezoelectric torque transducer for rheological measurements*

Conventional rotational rheometers utilize a torsion bar/spring or feedback servo to measure torque. Piezoelectric torque transducers have a much higher stiffness and resonance frequency than the conventional torque measurement techniques. Moreover, the current signal is proportional to the load that is applied over a wide range of torque values, and therefore, piezoelectric transducers are a favorable choice for taking rheological measurements, especially for the dynamic measurement. In this thesis, using a piezoelectric torque dynamometer in a rotational rheometer is reported for the first time and the applicability and suitability is validated.

ii. *Friction compensation for the increased torque limit*

The friction of the ball bearing and dynamic shaft seal often affects the accuracy and the lower limit of the torque measurement. In the developed rheometer, the friction of the dynamic seal significantly contributes to a large torque value, and this large torque value should be

compensated for. In the steady shear measurement, friction is significantly reduced by rotating the inner cylinder at a lower speed rather than jumping straight to the desired rate. Slowly rotating the inner cylinder removes the static friction, which is much larger than kinetic friction. In the sinusoidal oscillation mode, air torque is measured at each frequency and amplitude and directly subtracted from the measured value.

iii. *Flexibility of the system to perform various rheological measurements*

The developed rotational rheometer can be programmed to impose various strain histories, and this ability gives the rheometer flexibility to perform several rheological tests, more than has been reported in this thesis. Moreover, the torque transducer can almost instantaneously monitor and record the torque change without any issue of transducer inertia and compliance.

iv. *Reducing viscosity by dissolving gas under static pressure*

The viscosity of PDMS under various static pressures of CO_2 was experimentally determined. It was found that 3 MPa of CO_2 reduced the viscosity of PDMS by 45.6 % at 50°C compared to the atmospheric measurement. It was observed that 2 MPa of CO_2 reduced the viscosity of PDMS by 36.6% at 50°C. This result was similar to the result when the viscosity was reduced by increasing the temperature to 80°C (a 38.8% reduction).

v. *Development of a model that accounts for the effect of temperature and pressure*

An empirical model was developed to model the effect of temperature and CO_2 saturation pressure on the viscosity of PDMS. This model was based on the Doolittle's free volume concept, which expressed viscosity as function of free volume. Free volume was often calculated from the volumetric parameters of pure and mixture materials, which were difficult to obtain because of the complex thermodynamic concepts involved. In contrast, the developed model expresses free volume and viscosity as a direct function of temperature and pressure and is applicable in a

relatively low pressure range where Henry's law prevails. This model eliminates the need for difficult thermodynamic concepts and volumetric parameters of the material to estimate the viscosity of a material that contains dissolved gas.

5.3 Assumptions and Limitations

There are several assumptions and limitations in this study:

1. There is some eccentricity in the concentric cylinder due to the slight misalignment of the shaft and the dimensional inaccuracy of the machined parts. The eccentricity is worse at high rotational speeds due to the wobbling of the inner cylinder caused by the bearing clearance.
2. Excessive friction against the shaft seal reduces the performance and resolution of the developed rheometer. The friction compensation scheme proposed in this study requires laborious friction measurements under every operational condition including temperature, pressure, rotational speed, frequency, and amplitude. Moreover, friction can be affected by many factors including seal wear, shaft misalignment, and the presence of a fluid. The uncertainties in the friction results in the poor quality of the data, especially in the high pressure dynamic measurement.
3. The friction compensation scheme for the steady shear mode is valid only for the fluids that exhibit a Newtonian plateau region at a low shear rate.
4. Temperature is not directly measured in the fluid. Also, a temperature gradient within the fluid is ignored because the temperature is assumed to be constant throughout the sample.
5. The concentration of dissolved CO_2 could not be measured experimentally, but it was estimated from data in the literature.

6. It is assumed that the PDMS was fully saturated with CO_2 and that CO_2 was dissolved uniformly throughout the sample. In this study, 2 – 3 days were allowed for CO_2 to dissolve in the PDMS before the rheological measurements were taken. However, the saturation time could take up to few weeks or even months depending on the temperature.
7. The effect of pressure (without CO_2) on the viscosity was assumed to be negligible.

5.3 Future Work

Although the developed rheometer is somewhat limited in its performance and accuracy of measurement, it has the potential to be improved and to extend the range of operation. The piezoelectric torque dynamometer used in this study has a wide range of torque values ±100 Nm, which is approximately 500 times greater than that which the brushless DC motor can generate. Moreover, the natural frequency is more than 3000 Hz. Therefore, increasing the power of the motor will significantly increase the operational range of the rheometer.

The piezoelectric dynamometer is also capable of measuring the force in the z-axis. When a fluid that exhibits elasticity is sheared between cone-plate or parallel plate geometry, a force that pushes the plates apart is induced within the fluid in addition to the shear stress. This force is closely related to the first and second normal stress difference, which are other important rheological parameters.

The excessive friction experienced by the seal is the main obstacle that limits the accuracy of the measurements. Using a magnetic drive coupling instead of the dynamic seal will eliminate the uncertainty of measurement due to friction. In addition, the rheometer will be able to operate under much higher pressures without the possibility of the seal failing or leaking.

Although the rheological measurements were performed using PDMS-CO_2 in this research, other combinations of viscoelastic fluids and soluble gases can be used to investigate rheological measurements. For example, the effect of soluble gases on the rheology of bitumen can be studied. Moreover, the developed rheometer can also be used for in-situ monitoring of rheological changes during upgrading processes of bitumen.

REFERENCES

Areerat S, Nagata T, Ohshima M. 2002. Measurement and prediction of LDPE/CO2 solution viscosity. Polymer Engineering & Science 42:2234–2245.

Bae YC, Gulari E. 1997. Viscosity reduction of polymeric liquid by dissolved carbon dioxide. Journal of Applied Polymer Science 63:459–466.

Bagley EB. 1957. End Corrections in the Capillary Flow of Polyethylene. Journal of Applied Physics 28:624–627.

Barnes HA, Hutton JF, Walters K. 1991. An Introduction to Rheology. Elsevier, 1989.

Barus C. 1893. Isothermals, isopiestics and isometrics relative to viscosity. American Journal of Science s3-45:87–96.

Behzadfar E, Hatzikiriakos SG. 2013. Viscoelastic properties and constitutive modelling of bitumen. Fuel 108:391–399.

Calvet D, Wong JY, Giasson S. 2004. Rheological Monitoring of Polyacrylamide Gelation: Importance of Cross-Link Density and Temperature. Macromolecules 37:7762–7771.

Cox WP, Merz EH. 1958. Correlation of dynamic and steady flow viscosities. Journal of Polymer Science 28:619–622.

Doolittle AK. 1951. Studies in Newtonian Flow. II. The Dependence of the Viscosity of Liquids on Free-Space. Journal of Applied Physics 22:1471–1475.

Fujita H, Kishimoto A. 1958. Diffusion-controlled stress relaxation in polymers. II. Stress relaxation in swollen polymers. Journal of Polymer Science Part A: Polymer Chemistry 28:547–567.

Garg A, Gulari E, Manke CW. 1994. Thermodynamics of Polymer Melts Swollen with Supercritical Gases. Macromolecules 27:5643–5653.

Gerhardt LJ, Garg A, Manke CW, Gulari E. 1998. Concentration-dependent viscoelastic scaling models for polydimethysiloxane melts with dissolved carbon dioxide. Journal of Polymer Science Part B: Polymer Physics 36:1911–1918.

Gerhardt LJ, Manke CW, Gulari E. 1997. Rheology of polydimethylsiloxane swollen with supercritical carbon dioxide. Journal of Polymer Science Part B: Polymer Physics 35:523–534.

Ghannam MT, Esmail MN. 1998. Rheological Properties of Poly(dimethylsiloxane). Ind. Eng.

Chem. Res. 37:1335–1340.

Giacomin AJ, Samurkas T, Dealy JM. 1989. A novel sliding plate rheometer for molten plastics. Polymer Engineering & Science 29:499–504.

Jacobson B. 2003. The Stribeck memorial lecture. Tribology International 36:781–789.

Karmakar S, Kushwaha RL. 2007. Development and laboratory evaluation of a rheometer for soil visco-plastic parameters. Journal of Terramechanics 44:197–204.

Kelley FN, Bueche F. 1961. Viscosity and glass temperature relations for polymer-diluent systems. Journal of Polymer Science 50:549–556.

Khandare PM, Zondlo JW, Stansberry PB, Stiller AH. 2000a. Rheological investigation of pitch materials: Part I: Design and development of a high-temperature high-pressure (HTHP) rheometer. Carbon 38:881–887.

Khandare PM, Zondlo JW, Stansberry PB, Stiller AH. 2000b. Rheological investigations of pitch material: Part II: viscosity measurement of A240 and ARA-24 pitches using a high-temperature high-pressure rheometer. Carbon 38:889–897.

Kissi NE, Piau JM, Attane P, Turrel G. 1992. Shear rheometry of polydimethylsiloxane. Master curves and testing of Gleissle and Yamamoto relations. Elsevier.

Ladin D, Park CB, Park SS, Naguib HE, Cha SW. 2001. Study of shear and extensional viscosities of biodegradable PBS/CO_2 solutions. Journal of Cellular Plastics 37:109–148.

Lauger J. 2008. Thirteen years of EC-motors in rotational rheometers. Rio de Janeiro, Brazil. pp. 1–2; 2 p.

Lee M, Park CB, Tzoganakis C. 1999. Measurements and modeling of PS/supercritical CO_2 solution viscosities. Polymer Engineering & Science 39:99–109.

Macosko CW. 1996. Rheology: Principles, Measurements, and Applications; VCH: New York, 1994.

Marin G, Montfort JP. 1996. Molecular Rheology and linear viscoelasticity. Rheology Series 5:95–139.

Monnery WD, Svrcek WY, Mehrotra AK. 1995. Viscosity: A critical review of practical predictive and correlative methods. Can. J. Chem. Eng. 73:3–40.

Murata T, Date M, Kaibara M. 1987. Analysis of a Newly Developed Damped-Oscillation Rheometer: Newtonian Liquid. Japanese Journal of Applied Physics 26:1234–1240.

Oh J-H, Lindt JT. 2002. A Novel Couette Viscometer For Polymer Solutions in Supercritical Fluids. In Proceedings of SPE-ANTEC 2:1920–1923.

Pierre C, Barré L, Pina A, Moan M. 2004. Composition and heavy oil rheology. Oil and Gas Science and Technology 59:489–501.

Rabinowitsch B. 1929. Über die Viskosität und Elastizität von Solen. Zeitschrift für Physikalische Chemie 145A:1–26.

Rohn CL. 1995. Analytical Polymer Rheology: Structure-processing-property Relationships. Hanser.

Royer JR, DeSimone JM. 2001. High-pressure rheology and viscoelastic scaling predictions of polymer melts containing liquid and supercritical carbon dioxide. Journal of Polymer Science.

Royer JR, Desimone JM, Khan SA. 1999. Carbon Dioxide-Induced Swelling of Poly(dimethylsiloxane). Macromolecules 32:8965–8973.

Royer JR, Gay YJ, Adam M, DeSimone JM, Khan SA. 2002. Polymer melt rheology with high-pressure CO 2 using a novel magnetically levitated sphere rheometer. Polymer 43:2375–2383.

Royer JR, Gay YJ, Desimone JM, Khan SA. 2000. High-pressure rheology of polystyrene melts plasticized with CO2: Experimental measurement and predictive scaling relationships. Journal of Polymer Science Part B: Polymer Physics 38:3168–3180.

Smith FL, Harvey AH. 2007. Avoid common pitfalls when using Henry's law. Chemical engineering progress 103:33–39.

Williams ML, Landel RF, Ferry JD. 1955. The Temperature Dependence of Relaxation Mechanisms in Amorphous Polymers and Other Glass-forming Liquids. J. Am. Chem. Soc. 77:3701–3707.

Xu S, Wells PS, Tao Y, Yun KS, Parcher JF. 2009. Stationary- and Mobile-Phase Interactions in Supercritical Fluid Chromatography. In: Parcher JF; Chester TL, editors. Unified Chromatography, Copyright, Advisory Board, Foreword. Vol. 748. Washington, DC: American Chemical Society. (ACS Symposium Series). pp. 96–118; 23 p.

Yeo S-D, Kiran E. 1999. Viscosity Reduction of Polystyrene Solutions in Toluene with Supercritical Carbon Dioxide. Macromolecules 32:7325–7328.

Zener C. 1944. Anelasticity of Metals. The Journal of the Acoustical Society of America 16:100–100.

Intentionally left blank